Ba/Ca profiles in shells of Pecten maximus – A proxy for specific primary producers rather than bulk phytoplankton

Lukas Fröhlich, Valentin Siebert, Eric Walliser, Julien Thébault, Klaus Peter Jochum, Laurent Chauvaud, Bernd Schöne

Chemical Geology 593 (2022) 120743

Contents lists available at ScienceDirect

Chemical Geology

journal homepage: www.elsevier.com/locate/chemgeo

Ba/Ca profiles in shells of *Pecten maximus* – A proxy for specific primary producers rather than bulk phytoplankton

Lukas Fröhlich [a,*], Valentin Siebert [b], Eric O. Walliser [a,c], Julien Thébault [b], Klaus Peter Jochum [d], Laurent Chauvaud [b], Bernd R. Schöne [a]

[a] Institute of Geosciences, University of Mainz, Johann-Joachim-Becher-Weg 21, 55128 Mainz, Germany
[b] Univ Brest, CNRS, IRD, Ifremer, LEMAR, F-29280 Plouzané, France
[c] Museum Wiesbaden, Hessisches Landesmuseum für Kunst und Natur, Friedrich-Ebert-Allee 2, 65185 Wiesbaden, Germany
[d] Climate Geochemistry Department, Max Planck Institute for Chemistry, P.P. Box 3060, 55020 Mainz, Germany

ARTICLE INFO

Editor: Karen Johannesson

Keywords:
Phytoplankton
Sclerochronology
Diatoms
Bivalve mollusk
Environmental monitoring
Shells
Barium

ABSTRACT

Molar barium-to-calcium ratios in bivalve shells (Ba/Ca_{shell}) have been proposed in a variety of studies to serve as a potential proxy for the reconstruction of phytoplankton dynamics. However, the link between phytoplankton and Ba/Ca_{shell} profiles remains unclear and needs to be deciphered more accurately. In this study, we analyzed the relationship between Ba/Ca_{shell} peaks and specific phytoplankton species, and assessed the applicability of Ba/Ca_{shell} ratios as a species-specific phytoplankton proxy. The timing of peaks in highly resolved Ba/Ca_{shell} time-series in *Pecten maximus* shells (Bay of Brest, France) from two years (2011, 2012) were compared to the chlorophyll *a* concentration and the occurrence of individual diatom and dinoflagellate species. In addition, Monte Carlo simulations were used to approximate a species-specific contribution to the measured Ba/Ca_{shell} peaks. The results clearly demonstrated that the Ba/Ca_{shell} profiles cannot be explained either by the chlorophyll *a* concentration nor by the total diatom or dinoflagellate abundance. Instead, time-series of specific phytoplankton, especially diatoms, revealed a high degree of synchronicity with Ba/Ca_{shell} peaks when temporally lagged by 8 to 13 days (depending on species). The Monte Carlo simulations suggested that the Ba/Ca_{shell} peak heights cannot be fully explained by the observed phytoplankton cell concentration, but rather by individually weighted phytoplankton time-series, most likely caused by inter-species differences such as cell size and chemical ability to adsorb Ba. Moreover, the approximated species-specific weighting factors agreed well between the studied years. According to our findings, Ba/Ca_{shell} peaks are likely associated with blooms of specific phytoplankton taxa, with a time lag of ca. one to two weeks, and the amount of cell-associated Ba varies between phytoplankton species. These conclusions provide further insights into the formation of Ba enrichments in bivalve shells and improves the applicability of Ba/Ca_{shell} profiles as a species-specific proxy of past phytoplankton dynamics.

1. Introduction

Marine phytoplankton plays a crucial role in the global net primary production (Field et al., 1998; Westberry et al., 2008). It also contributes significantly to the photosynthetic fixation and regulation of atmospheric CO_2 (Iglesias-Rodriguez et al., 2008; Shuter, 1979; Sigman and Boyle, 2000) and oxygen production (Field et al., 1998), and serves as the basis of the marine food web. Changing environmental conditions such as climate warming (Barton et al., 2020; Winder and Sommer, 2012), ocean acidification (Iglesias-Rodriguez et al., 2008) or nutrient input by artificial fertilizers (Beman et al., 2005; Del Amo et al., 1997) can lead to a shift in the phytoplankton community composition (Behl et al., 2011). Shifting community structures in turn can have important consequences for climate and ecosystems (Cardinale et al., 2006; Worm et al., 2006) and impact commercial fisheries because of eutrophication and harmful algae blooms (Liu et al., 2008; Ragueneau et al., 2002; Shumway and Cembella, 1993; Smith, 2003). To better understand long-term repercussions of changes in phytoplankton species composition it is necessary to gain a better comprehension of past phytoplankton dynamics. This includes insights into changes of the primary producer

* Corresponding author.
E-mail address: lufroehl@uni-mainz.de (L. Fröhlich).

https://doi.org/10.1016/j.chemgeo.2022.120743
Received 12 August 2021; Received in revised form 25 January 2022; Accepted 27 January 2022
Available online 2 February 2022

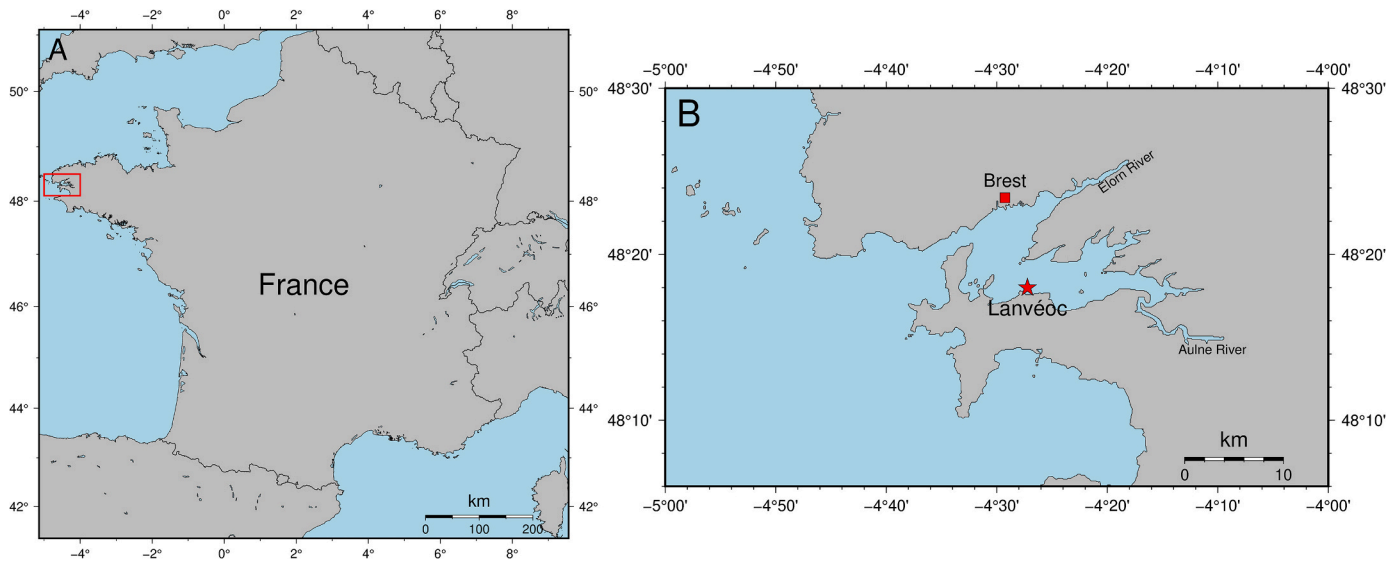

Fig. 1. A) Map of France and the study site (Bay of Brest) marked with a red rectangle. B) Magnification of the Bay of Brest showing the sampling locality (Lanvéoc, red star). (For interpretation of the references to colour in this figure legend, the reader is referred to the web version of this article.)

community structures through time and space.

Continuous and highly resolved primary production records are only available since a few decades and for a few localities (e.g., Richardson and Heilmann, 1995; Lindahl et al., 1998; Chauvaud et al., 2000; Cadée and Hegeman, 2002). However, this time interval is too short to reliably identify long-term changes in global phytoplankton dynamics and evaluate the anthropogenic impact (Henson et al., 2010). Therefore, different past marine primary production data were reconstructed from various proxies (Anderson and Winckler, 2005; Averyt and Paytan, 2004) such as the amount of barite in marine sediments that is linked to the decay of phytoplankton cells (Bishop, 1988; Dehairs et al., 1980; Ganeshram et al., 2003), foraminiferal assemblages (Herguera, 2000; Herguera and Berger, 1991) as well as Ba/Ti and Al/Ti ratios of bulk sediments (Dymond et al., 1997). Although marine sediment cores provide long-term archives, covering several thousands of years (e.g., Cheshire et al., 2005), the low accumulation rates prevent gaining a high temporal resolution. This prohibits a detailed reconstruction of short-term events, on a daily to weekly scale, of past phytoplankton dynamics. Instead, shells of bivalves potentially serve as an alternative high-resolution, temporally well-constrained archive of primary production. Bivalve mollusks precipitate their shell periodically (Hallmann et al., 2008; Richardson et al., 1980; Schöne, 2008) resulting in distinct growth patterns, i.e., daily, fortnightly and annual growth lines. These growth increments (periods of slow and fast growth, respectively) can be used to place the shell record into a precise temporal context. During growth, bivalves record environmental changes in the form of variable increment widths and chemical properties. According to previous studies of different bivalve species, barium-to-calcium ratios of the shell (Ba/Ca_{shell}) potentially serve as a proxy for primary production in marine settings (Barats et al., 2009; Doré et al., 2020; Gillikin et al., 2006; Lazareth et al., 2003; Marali et al., 2017a, 2017b; Stecher et al., 1996; Thébault et al., 2009; Vander Putten et al., 2000). A common pattern of Ba/Ca_{shell} ratios in bivalves includes a relatively stable and low background signal interrupted by sharp Ba/Ca_{shell} peaks (Barats et al., 2009; Gillikin et al., 2008; Hatch et al., 2013; Marali et al., 2017a; Thébault et al., 2009). Since the Ba/Ca_{shell} profiles of contemporaneous shells from the same population are highly synchronous (Barats et al., 2009; Doré et al., 2020; Gillikin et al., 2008; Marali et al., 2017a, 2017b; Thébault et al., 2009), a common environmental forcing is likely (Carré et al., 2006; Gillikin et al., 2008; Hatch et al., 2013; Vander Putten et al., 2000). Although a general consensus exists regarding the cause of the stable background signal, it most likely reflects the Ba/Ca ratio of the seawater (Barats et al., 2009; Gillikin et al., 2008, 2006), different hypotheses emerged concerning the sharp Ba/Ca_{shell} peaks, which cannot be adequately explained by variations in the dissolved barium concentration of the surrounding medium (Barats et al., 2009; Gillikin et al., 2008). It is possible that bivalves ingest barite crystals induced by the decomposition of large amounts of phytoplankton cells following blooms (Bishop, 1988; Ganeshram et al., 2003; Stecher et al., 1996; Stecher and Kogut, 1999), leading to the desorption of barium in their gut and followed by the incorporation of barium into the shell carbonate (Takesue et al., 2008). However, it appears more likely that the direct ingestion of phytoplankton cells enriched in barium lead to the formation of Ba/Ca_{shell} peaks, because the ingestion of barite particles insufficiently explains the Ba/Ca_{shell} time-series in pectinids (Thébault et al., 2009). Previous studies demonstrated a large variability in the barium concentration between various marine phytoplankton species (Fisher et al., 1991; Martin and Knauer, 1973; Roth and Riley, 1971). Furthermore, according to Sternberg et al. (2005), barium is precipitated onto diatom frustules via the adsorption onto iron oxyhydroxides. Since a direct link between Ba/Ca_{shell} profiles and phytoplankton biomass could not be established in previous studies (Barats et al., 2009; Gillikin et al., 2008; Thébault et al., 2009), detailed analyses are required to decipher a potential relation between Ba/Ca_{shell} peaks and phytoplankton dynamics on a species level.

The goal of this study is to refine knowledge about Ba/Ca_{shell} profiles from bivalve shells and the interconnection with phytoplankton in coastal ecosystems. To evaluate this relationship, shells of the short-lived bivalve, *Pecten maximus,* serve as an ideal geochemical archive as they provide growth increments that are formed on a daily basis (Chauvaud et al., 1998) which in turn allows to extract daily resolved Ba/Ca_{shell} time-series. This high-temporal resolution is necessary in order to reconstruct primary producer dynamics, such as efflorescence, which is ephemeral and occurs over a short period of time. This study compares highly resolved phytoplankton observations with temporally contextualized Ba/Ca_{shell} profiles. The following questions will be addressed herein: (1) Does a direct relationship exist between the bulk phytoplankton in the water column and Ba/Ca_{shell} profiles? (2) Can the timing and magnitude of Ba/Ca_{shell} peaks be used to interpret past phytoplankton dynamics? (3) Is there a species-specific contribution of phytoplankton to the Ba/Ca_{shell} profile? Diatoms and dinoflagellates constitute the main phytoplankton groups in the studied coastal area and were used together with the chlorophyll *a* concentration (a rough gauge of the bulk phytoplankton biomass) to address these questions. To

Table 1
Overview of specimens analyzed in this study for barium content by means of LA-ICP-MS. LOD = Limit of detection (LOD). Relative standard deviations (RSD) were calculated from repeated measurements of the external standard material NIST SRM 612. For quality control, the average concentrations and standard deviations (± 1σ) for blind measurements of the synthetic carbonate reference material USGS MACS-3 are given and compared with a reference value (59.6 ± 1.4 μg g^{-1}) provided by the GeoReM database (http://georem.mpch-mainz.gwdg.de/). Differences between measured MACS-3 values and the literature value vary between 1.4% to 12.2%.

Sample ID	Date of collection	LOD (mmol mol^{-1})	RSD (%)	Concurrently analyzed MACS-3 values (μg g^{-1})
Shell A	30 August 2011	9×10^{-6}	2.0	56.6 ± 4.8
Shell B	30 August 2011	1×10^{-5}	1.7	65.6 ± 4.3
Shell C	30 August 2011	8×10^{-6}	2.6	54.8 ± 4.6
Shell D	23 October 2012	9×10^{-6}	5.5	66.9 ± 4.0
Shell E	23 October 2012	5×10^{-6}	3.1	58.8 ± 2.5
Shell F	23 October 2012	1×10^{-5}	2.5	66.2 ± 5.8

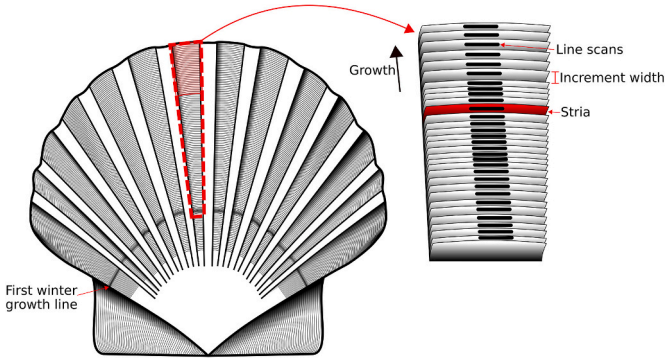

Fig. 2. Schematic illustration of the left valve of an age class 1 specimen (*P. maximus*) showing one annual growth line. Dashed red line represents the extracted shell portion of an indented valley that is located between radial ribs. LA-ICP-MS measurements were performed on this shell portion. The magnification (right panel) displays daily formed increments (distance between two successively formed striae) on the external shell surface. The distance between successive growth striae was used to determine the growth rate of the shell. The thick black markers indicate the LA-ICP-MS sampling, i.e., line scans that were conducted on each growth increment. The direction of growth is indicated as a black arrow. (For interpretation of the references to colour in this figure legend, the reader is referred to the web version of this article.)

substantiate possible relationships between phytoplankton and the shell chemistry, a special focus was placed on the timing and magnitude of Ba/Ca_{shell} enrichments and phytoplankton blooms. Deciphering this linkage will promote the applicability of Ba/Ca_{shell} profiles as a valuable proxy for past phytoplankton dynamics.

2. Material and methods

2.1. Study site and sample preparation

A total of six specimens of *P. maximus* were collected alive at a depth of about 8 m by SCUBA diving at Lanvéoc (48°17′N 4°30′W), Bay of Brest, Brittany, northwest France (Fig. 1). The Bay of Brest is a semi-enclosed coastal ecosystem (180 km^2) with an average depth of 8 m. The sampling site, Lanvéoc, is located in the southern part of the bay. Three specimens were obtained on 30 August 2011 and another three on 23 October 2012 (Table 1). Shells of all studied specimens showed one winter growth line and are therefore referred to as age-class 1 shells. Immediately after collection, the specimens were stored in the freezer at −20 °C. *Prior* to sclerochonological analysis, the bivalves were eviscerated and epibionts were removed. Following previous studies (e.g., Chauvaud et al., 1998, 2011; Jolivet et al., 2015; Marchais et al., 2015), the left (flat) valves were used for element chemical and growth pattern analyses (Fig. 2). In order to clean the surface of the shells (outer shell layer made of calcite), remove the periostracum and adhering sediment that was trapped between adjacent striae, the valves were gently cleaned using a plastic brush, followed by 3 min ultrasonication in deionized water. In advance of chemical analyses, further cleaning steps were applied (see section 2.3).

2.2. Growth pattern analysis and temporal alignment

For growth pattern analysis, photographs (e.g., see Supplementary Fig. S1) were taken on the outer surface of the shells within the depression between radiating ribs along the axis of maximum growth (Fig. 2), more specifically, the portion between the first winter line and the ventral margin. For this purpose, a Canon EOS 600 DSLR camera was coupled to a Wild Heerbrugg binocular microscope equipped with a Schott VisiLED MC 1000 light source (sectoral dark field). Overlapping images were stitched together using the Image Composite Editor software (version 2.0.3.0) provided as freeware by the Microsoft Research Computational Photography Group.

The daily formed microgrowth increments and lines (called striae) of *P. maximus* can be used to place the shell growth record including geochemical data into a precise temporal context. If the date of collection is known, exact calendar days can be assigned to each microgrowth increment (e.g., Chauvaud et al., 1998; Lorrain et al., 2004; Gillikin et al., 2008). This is accomplished by counting the striae from the ventral margin (most recently formed shell portion) toward the umbo. Increment widths were determined by measuring the distance between adjacent striae following the method described by Chauvaud et al. (1998). Shell growth rates are given in μm day^{-1}. Growth curves of different contemporaneous specimens were then crossdated by wiggle-matching and minimizing the sum of least squares. As previously demonstrated by Thébault et al. (2006, 2009) for the pectinid shells, *C. radula*, the visual determination of successive striae is not always unambiguous (i.e., because of slightly fractured shell portions, overlapping striae or barely visible striae) leading to a subjective, inter-reader difference. The inter-reader discrepancies in striae determination in *P. maximus* shells were calculated from differences in repeated counts and measurements of daily formed striae performed by different readers ($n = 3$) and expressed as the relative standard deviation (RSD%). In this study, the inter-reader differences remain low (RSD% of 0.67%), i.e., solely a small uncertainty (± 2 days) in the growth reading process and thus, in the temporal assignment of the geochemical data, has to be considered.

2.3. LA-ICP-MS analysis

In preparation for chemical analysis, the portion used for growth pattern analysis was cut from each shell (Fig. 2) using a 150 μm-thin diamond disk (disk with galvanically bonded diamonds; Komet – Dental Gebr. Brasseler GmbH & Co. KG; Art.-No.: 6911H.-104.220) mounted to a handheld drill. To remove potential surface contaminants, the shell slab was soaked in acetic acid (10 vol%) for ca. 1 min. Followed by rinsing in deionized water. Since the studied species attains its maximum annual increment width between the 1st and 2nd winter growth stops in scallop populations from the Bay of Brest, chemical analyses provided a nearly daily resolution.

Geochemical analyses were performed with a Laser Ablation – Inductively Coupled Plasma – Mass Spectrometer (LA-ICP-MS) system at the Max Planck Institute for Chemistry (Mainz, Germany). In total, six

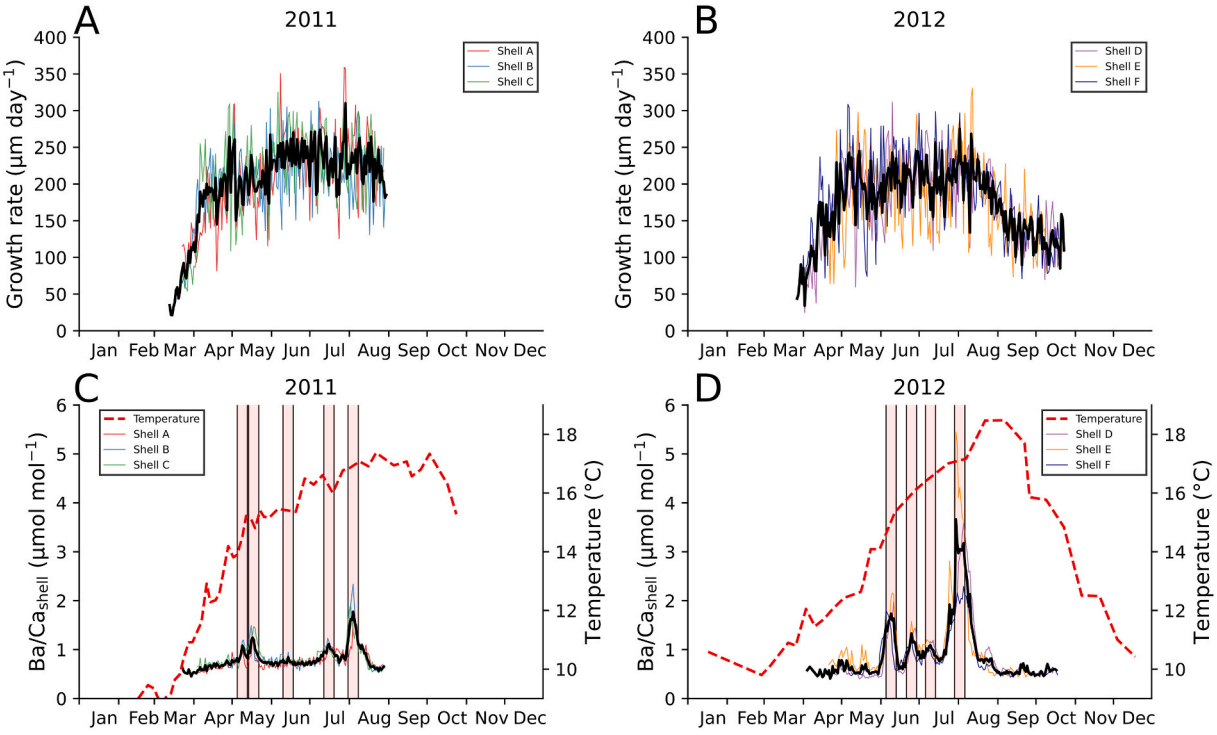

Fig. 3. Growth rates of three age class 1 specimens from 2011 (A) and 2012 (B). The Ba/Ca$_{shell}$ data of each specimen (C, D) were temporally aligned by counting daily growth increments from the date of collection. Black lines represent arithmetic means of shell growth rates and Ba/Ca$_{shell}$ values for the three studied specimens in the respective year. Ba/Ca$_{shell}$ peaks (see Table 2 for the exact peak position) are highlighted in red for better visual detection (peak position ±4 days). In addition, the water surface temperature measured at the site of shell collection is shown (C, D). (For interpretation of the references to colour in this figure legend, the reader is referred to the web version of this article.)

shell slabs (three from 2011 and three from 2012) were analyzed for their barium (using ^{137}Ba as analyte) content. Laser scans were completed on the striae, by running the laser in line scan mode on the outer shell surface perpendicular to the growth direction and parallel to the striae (Fig. 2). Within each stria, measurements were completed with a laser spot diameter of 80 µm at a constant speed of 5 µm s^{-1}. Each scan was 600 µm long. Where possible, every daily stria was sampled (Fig. 2), unless the stria width was narrower than 80 µm (smaller than the laser spot size). Prior to sample ablation and measurement, each sample was pre-ablated (100 µm spot size, 80 µm s^{-1}) to remove potential contaminants. According to previous in-situ chemical analyses (Barats et al., 2007), trace elements are homogeneously distributed within single striae of *P. maximus*. Thus, measured signal intensities were averaged for each line scan. For consistency, reference materials used for calibration and quality control were ablated in the same manner. The ablation was performed with a NewWave Research UP-213 Nd:YAG laser ablation system (New Wave Research, Fremont, CA, USA) at a repetition rate of 10 Hz and a laser energy density of 15.8 J cm^{-2} with helium as an initial carrier gas (quality 5.0, flow rate 0.57 L min^{-1}). The ion intensities were measured with a Thermo Fisher Element 2 single collector sector-field ICP-MS (Thermo Fisher Scientific, Bremen, Germany) coupled to the laser system, using argon as a carrier gas (quality 5.0, flow rate 0.77 L min^{-1}). The reference material NIST SRM, a synthetic silicate glass, was used as an external standard (values obtained from the GeoReM database; http://georem.mpch-mainz.gwdg.de/; last access: 18 March 2021; 612 Jochum et al. (2011)) and ^{43}Ca was used as an internal standard to normalize obtained barium signal intensities.

A Microsoft Excel spreadsheet was used for data reduction, following the calculations provided by Longerich et al. (1996) and Jochum et al. (2007, 2011). Blanks were determined 15 s prior to ablation. Detection limits were calculated based on the 3σ criterion. All detection limits (Table 1) were significantly lower than the Ba/Ca$_{shell}$ signal, with an average limit of detection of 9 × 10^{-6} mmol mol^{-1}. To account for uncertainties of reproducibility, the relative standard deviation in percent (RSD%) was calculated from repeated measurements of the NIST SRM 612 reference material. For Ba, an average RSD% value of 2.9% was obtained (Table 1). The synthetic carbonate USGS MACS-3, a pressed powder pellet, was used for quality control. Measured Ba concentrations of USGS MACS-3 differed by 1.4 to 12.2% from the published reference value (GeoReM database; Table 1). High deviations from the reference value might be induced by changing ablation behavior due to varying particle sizes of the MACS-3 carbonate pellet leading to differences in ionization and uncertainties of the non-certified MACS-3 reference material (Jochum et al., 2019).

2.4. Environmental parameters

To determine the species composition of phytoplankton and chlorophyll *a* concentration at Lanvéoc (Fig. 1; similar sampling site as shell collection), seawater was collected during daytime (within a 3-h window before or after high tide) using a 5 L Niskin bottle that was positioned vertically in the water column approx. 1.5 m below the water surface. In 2011, seawater was sampled once a week between January – March and July – October and twice per week from April until June. In 2012, samples were taken once a week between March and May, and biweekly between June and December. This resulted in 52 water samples collected during 2011 and 26 samples in 2012 (Supplementary Table S1). Each water sample (250 mL) was filled in a vial using a silicone tube that was in contact with the bottom of the bottle to avoid turbulence within the sample and to prevent the phytoplankton cells from disintegration. The phytoplankton cells were fixed with 2.5 mL of Lugol's solution and transported to the laboratory within one hour after sampling. Until further analyses, the samples were stored in a dark place to prevent the alteration of the cells by UV radiation. To determine the phytoplankton species and abundance, 50 mL of the sample was filled into a sedimentation column and left for 24 h to let the phytoplankton

cells settle down onto a microscope glass slide. The species determination and the cell counting were performed by observing the recovered glass slide with an inverted microscope (Axio Observer.A1-ZEISS, Carl Zeiss MicroImaging GmbH, Göttingen, Germany). Phytoplankton cell abundances are given in cells L^{-1}. Hereafter, the short-term increase in cell concentration of a specific phytoplankton species is referred to as a phytoplankton peak or bloom, i.e., clearly observable maxima in the cell concentration time-series (see Supplementary Fig. S2 and S3). Water samples were analyzed for their chlorophyll *a* concentration by filtering the water with glass fiber filters (GF/F Whatman). Chlorophyll *a* pigments were then extracted using 6 mL of 90% acetone and stored in the dark for 12 h at 4 °C, followed by two episodes of centrifugation (for 5 and 10 min at 3000 rpm) and fluorescence measurement with a Turner Design fluorometer. The chlorophyll *a* concentration was then calculated based on the equation of Lorenzen (1966).

2.5. Timing of phytoplankton blooms and Ba/Ca_{shell} peaks

To evaluate the possible relationship between phytoplankton cells in the water column and exceptionally high Ba/Ca_{shell} values in *P. maximus*, the timing of blooms of different phytoplankton species was compared to the timing of Ba/Ca_{shell} peaks. Since previous studies observed a temporal lag between environmental changes, such as chlorophyll *a* peaks or phytoplankton blooms, and the occurrence of transient Ba/Ca_{shell} peaks (e.g., Barats et al., 2009; Thébault et al., 2009), the following method was used to account for this eventual temporal offset. The temporal alignment of the barium peaks was accomplished by growth pattern analysis (see section 2.2). To define a narrow temporal time frame for each distinct Ba/Ca_{shell} peak, a time interval of ±4 days was assigned for each peak (see Fig. 3; red areas). This time interval was determined in order to fulfill the following purposes: (1) Since small inter-shell variations in the absolute timing of Ba/Ca_{shell} peaks of contemporaneous specimens exist (e.g., the temporal occurrence of last Ba/Ca_{shell} peaks in shell E and shell D differ about 7 days), this time interval ensures to enclose all simultaneously occurring Ba/Ca_{shell} peaks. (2) The time interval considers a small uncertainty yielded by the temporal alignment of the geochemical data (see section 2.2). (3) For the comparison between timing of Ba/Ca_{shell} peaks and species-specific phytoplankton cell concentration time-series, the assigned time intervals serve as a clearly defined time frame that allows to explicitly identify time lags between a phytoplankton bloom and the occurrence of a Ba/Ca_{shell} peak.

To determine the time lag between the occurrence of blooms of specific phytoplankton cells and Ba/Ca_{shell} peaks, each phytoplankton time-series was shifted manually relative to the Ba/Ca_{shell} time-series until peaks overlapped, i.e., peaks in the phytoplankton time-series fell in the Ba/Ca_{shell} time interval (see Supplementary Fig. S2, S3). For the ease of analyzing the various phytoplankton time-series, studied phytoplankton species were classified into four categories, based on their agreement with Ba/Ca_{shell} peaks (without considering physiological characteristics). Phytoplankton time-series that were assigned to category 1 provided a distinct time lag so that all cell concentration peaks coincided to a Ba/Ca_{shell} peak. Time-series of category 2 denoted species that cell concentration peaked multiple times throughout the year, but not all phytoplankton peaks (or just minor peaks) matched with Ba/Ca_{shell} excursions after shifting the time-series with a certain temporal lag. Phytoplankton time-series were assigned to category 3 if the peaks occurred more than 30 days before the Ba/Ca_{shell} peaks, or after the last Ba/Ca_{shell} peak. All remaining species correspond to category 4 indicating that no running similarity exists between the chronologies. Consequently, species-specific time lags could only be determined for phytoplankton time-series of category 1 and 2.

2.6. Evaluation of the relationship between individual phytoplankton species and Ba/Ca_{shell} using pseudo-random sampling simulations

Since it was impractical to measure the barium content of individual phytoplankton cells in the studied years, the Ba/Ca_{shell} peaks were approximated by applying a specific weighting factor to individual diatom and dinoflagellate cell concentration time-series generated by Monte Carlo simulations. The aim of this approach is to numerically analyze complex systems such as the potential relationship between Ba-associated phytoplankton cells of various species and the formation of Ba/Ca_{shell} peaks. The immense number of possibilities makes it nearly impossible to determine a theoretical factor that optimally describes the relative amount of cell-associated Ba for each phytoplankton taxon and how it contributes to the measured Ba/Ca_{shell} chronologies. The Monte Carlo method iteratively tests billions of possible scenarios by using randomly generated parameters (i.e., differently weighted phytoplankton time-series). Within each simulation, a randomly selected weighting factor (between 0 and 100) was assigned to each phytoplankton time-series that was included in the respective simulation. All time-series were temporally shifted by a previously determined time lag (see section 2.5). In addition, the randomly obtained values were used to assign a weight to the individual time-series by multiplying the cell concentration data with the respective weighting factor (Supplementary Fig. S4). For each simulation, the weighted cell concentration data of the different phytoplankton taxa were then combined to a new time-series and compared to the Ba/Ca_{shell} profile of the respective year by calculating the Pearson correlation coefficient. Each run consisted of 10^8 simulations, where the simulation with the largest Pearson correlation coefficient constituted the result of the run (see Appendix A). Sixteen different phytoplankton species were included in the simulation for 2011, and fifteen for 2012. In total, 50 runs with 5 billion tested combinations were performed for each year. Based on this large number of repetitions, a pattern could be derived that provided information about the potential species-specific contribution to the Ba/Ca_{shell} profile. The underlying assumptions for this random sampling approach were: (1) All included phytoplankton species can potentially be ingested and digested by the bivalves. (2) There is no pre-digestive selection preference of individual phytoplankton species by the scallops, i.e., all phytoplankton cells were ingested and digested proportionally to the number of cells in the water column. (3) Cells of different phytoplankton species can contain different amounts of Ba that will end up in the shell.

3. Results

3.1. Shell growth patterns and Ba/Ca_{shell} profiles of *P. maximus*

Within the same calendar year, daily increment width chronologies of the studied specimens showed a high degree of synchronicity (Fig. 3). The general pattern of seasonal growth during the two studied years also compared well to each other (Fig. 3). Annual growth lines were formed between November and March. Daily growth rates increased gradually from late March (20 to 60 μm day^{-1}) to the beginning of May. As revealed by daily growth pattern analysis, the period of maximum growth (between May and late August) of the studied *P. maximus* specimens comprised ca. 121 ± 2 days, with growth rates between 130 and 150 μm day^{-1} in 2011 and 130 and 280 μm day^{-1} in 2012 (Fig. 3A, B). After the end of August, growth rates declined until the date of collection (Fig. 3A, B).

Similar to the daily growth curves, Ba/Ca_{shell} chronologies of contemporaneous specimens agreed well with each other and exhibited a strong reproducibility (Fig. 3C, D). Pearson correlation coefficients ($p < 0.05$) ranged between 0.58 (shell A vs shell C) and 0.78 (shell B vs shell C) for 2011 and between 0.82 (shell D vs shell E) and 0.89 (shell D vs shell F) for 2012. In general, the Ba/Ca_{shell} profiles were characterized by a constant background level (2011: 0.63 ± 0.06 μmol mol^{-1}; 2012: 0.56 ± 0.06 μmol mol^{-1}) that was occasionally interrupted by sharp Ba/

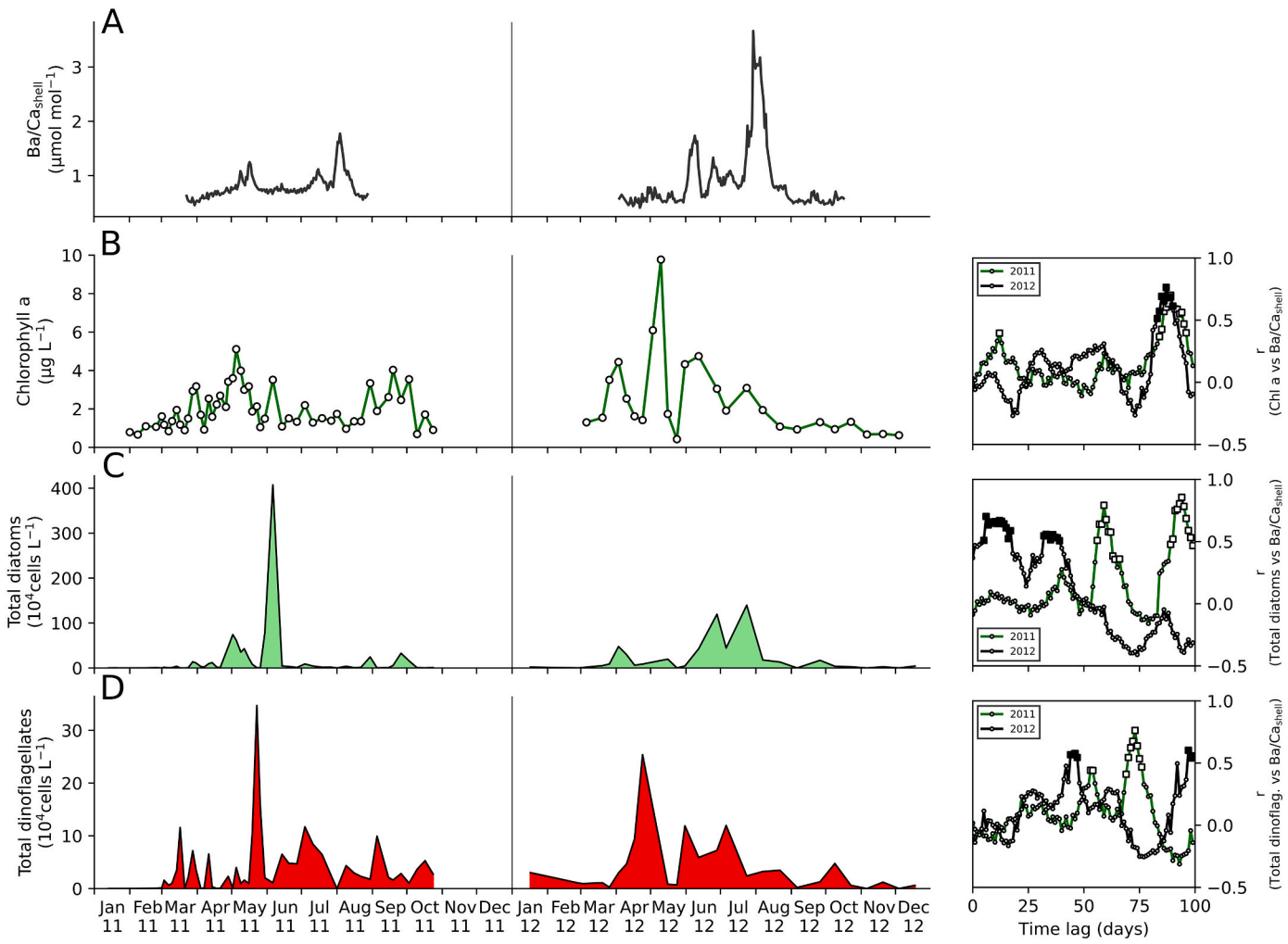

Fig. 4. Variations in Ba/Ca$_{shell}$ in shells from *P. maximus* (A), in chlorophyll *a* (B), total diatoms cell counts (C) and total dinoflagellate cell counts (D) at Lanvéoc during 2011 and 2012. Diagrams to the right display the Pearson correlation coefficients (*r*) calculated between the respective environmental parameter and the measured Ba/Ca$_{shell}$ profiles for lags of 0 to 100 days. Statistically significant correlations (with $p < 0.05$) are depicted as solid squares.

Table 2
Determined Ba/Ca$_{shell}$ maxima in *P. maximus* shells from 2011 and 2012 and their respective temporal occurrence within the shell chronology.

	2011		2012	
Peak #	Date	Ba/Ca$_{shell}$ (µmol mol^{-1})	Date	Ba/Ca$_{shell}$ (µmol mol^{-1})
Peak 1	05 May to 13 May	1.08	05 June to 13 June	1.73
Peak 2	14 May to 22 May	1.24	21 June to 29 June	1.33
Peak 3	10 June to 18 June	0.84	06 July to 14 July	1.08
Peak 4	12 July to 20 July	1.11	29 July to 06 August	3.66
Peak 5	31 July to 08 August	1.77		

Ca$_{shell}$ peaks (Fig. 3C, D, 4A). Despite the high Ba/Ca$_{shell}$ reproducibility within the same calendar year, Ba/Ca$_{shell}$ trajectories of the three shells from 2011 differed strongly from those of 2012. Five Ba/Ca$_{shell}$ peaks were identified in the specimens from 2011 (Fig. 3C; Table 2) with average Ba/Ca$_{shell}$ peak heights varying between 0.84 and 1.77 µmol mol^{-1}. The Ba/Ca$_{shell}$ profiles from 2012 revealed four distinct maxima (Fig. 3D, Table 2), with peak heights ranging between 1.08 and 3.66 µmol mol^{-1}. Notably, in both studied years, strong Ba/Ca$_{shell}$ excursions were missing at the beginning of the growing season, i.e., between March and May (Fig. 3C, D; Table 2).

3.2. Phytoplankton dynamics and seawater temperature

In 2011, the chlorophyll *a* concentration varied between 0.67 µg L^{-1} in February and 5.11 µg L^{-1} in May (Fig. 4B), with an average of 1.99 ± 1.04 µg L^{-1}. The highest chlorophyll *a* values corresponded to a diatom peak (approx. 742,500 cells L^{-1}) recorded on 2 May 2011 (referred here to as 'spring diatom bloom'). However, a much larger diatom bloom (maximum approx. 4,072,860 cells L^{-1}) that occurred on 6 June and lasted 19 days ('summer diatom bloom') was only associated with a smaller peak in chlorophyll *a* (Fig. 4B, C). Two smaller diatom blooms evolved during the end of August and the end of September 2011 with 244,640 and 327,300 cells L^{-1}, respectively. The largest number of dinoflagellates (approx. 347,080 cells L^{-1}) was recorded on 23 May, i.e., after the diatom spring bloom and prior to the summer diatom bloom (Fig. 4D). This dinoflagellate bloom was the largest of both studied calendar years. In addition, 11 smaller dinoflagellate peaks (on average 65,714 cells L^{-1}) occurred throughout 2011. During 2011, 25 different types of diatoms, with blooms containing more than 1000 cells L^{-1}, were identified in the surface water (Supplementary Table S3). By far, the most abundant diatom taxon (79.10% of total diatom cells) belonged to single, isolated cells of the genus *Chaetoceros* (Supplementary Table S3) and made up nearly 30% of the total phytoplankton cells at Lanvéoc. The largest bloom of *Chaetoceros* spp. emerged between 26 May and 13 June

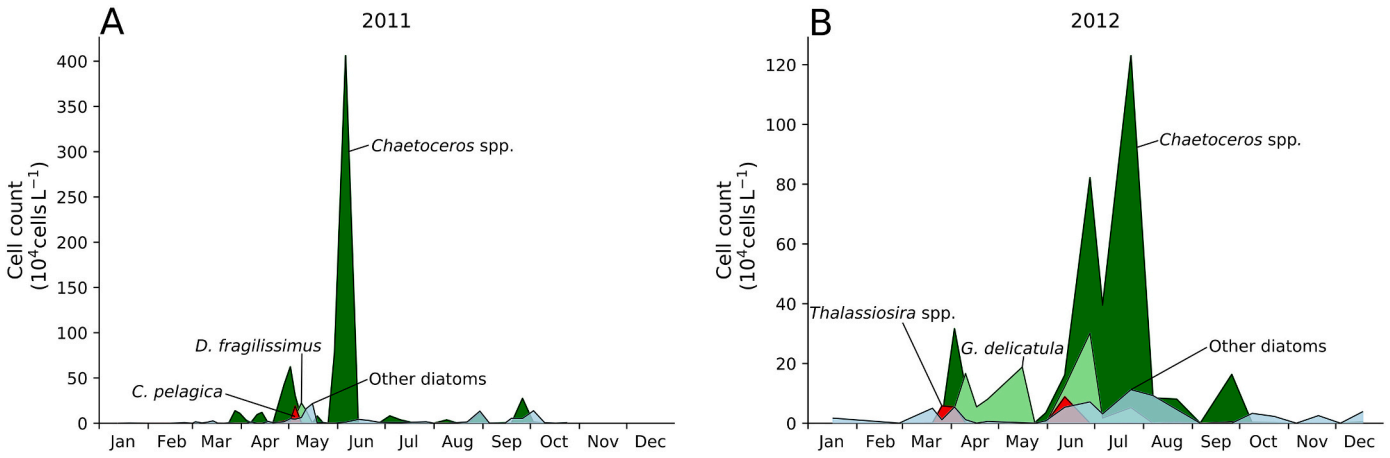

Fig. 5. Temporal distribution and cell concentration of the three most abundant diatom species (*Chaetoceros* spp., *Dactyliosolen fragilissimus* and *Cerataulina pelagica*) and the sum of 23 minor diatoms at Lanvéoc during 2011 (A). The temporal variations in cell counts of *Chaetoceros* spp., *Thalassiosira* spp., *Guinardia delicatula* and the sum of 20 minor diatoms in 2012 (B). Species names of minor diatoms are given in Table S3 (Supplementary) for 2011 and Table S5 (Supplementary) for 2012. Note different scaling of y-axes in A and B.

(Fig. 5A). During the decline of the *Chaetoceros* spp. cells around 8 May, two other diatom species started to grow, which made up the second and third most abundant diatoms in 2011, i.e., *Dactyliosolen fragilissimus* and *Cerataulina pelagica* (Supplementary Table S3; Fig. 5A). The lower abundances of *D. fragilissimus* around 12 May potentially promoted the formation of blooms composed of minor diatom species (Supplementary Table S3; Fig. 5A). After the large summer bloom, only smaller diatom blooms occurred until the end of September. Then, *Chaetoceros* spp. growth restarted concomitantly with blooms of other, less abundant diatom species. The most abundant dinoflagellates belonged to the species *Heterocapsa minima* and *Gymnodinium* sp. (with cell size >20 μm), which presented 80% of the total dinoflagellate cells (Supplementary Table S4). However, these dinoflagellates contributed only to a small extent (6.13%) to the total phytoplankton cells that were observed in 2011. The largest bloom of *H. minima* occurred around 23 May, i.e., between the largest diatom blooms (Fig. 4C, D). In general, blooms of dinoflagellate species emerged more frequently throughout the year (e.g., cell counts of *Gymnodinium* sp. peaked 13 times in 2011) in comparison to diatom species, though to a smaller extent.

In 2012, the chlorophyll *a* concentration fluctuated between 0.43 in late May and 9.77 μg L^{-1} in early May with a mean concentration of 2.44 ± 2.13 μg L^{-1} (Fig. 4B). Two diatom peaks occurred at 28 June (821,830 cells L^{-1}) and 24 July (1,230,000 cells L^{-1}) that corresponded to contemporaneous elevations in chlorophyll *a* (Fig. 4C). However, the largest chlorophyll *a* concentration of 10 May did not coincide with seasonal diatom growth peak. Three main dinoflagellate blooms (up to 253,960 cells L^{-1}) occurred on 24 April, 3 May and 6 July (Fig. 4D), i.e., during time intervals of relative low diatom abundance. Similar to 2011, diatoms were dominated by *Chaetoceros* spp. (Fig. 5B, Supplementary Table S5) which contributed to 63.65% to the total amount of diatom cells in 2012. Three *Chaetoceros* spp. blooms emerged on 24 July, 28 June and 3 April. *Guinardia delicatula* and cells of the genus *Thalassiosira* made up the second and third most abundant diatoms that were present during 2012 and peaked concomitantly with the second *Chaetoceros* spp. bloom. Between mid-April and June, the diatom *G. delicatula* clearly dominated the phytoplankton community and reached a maximum on May 16 (187,770 cells L^{-1}; Fig. 5B). In addition, 20 minor diatom species were identified with peaks containing more than 1000 cells L^{-1} (Supplementary Table S5). Dinoflagellates were mostly represented by *Gymnodinium* sp. (with cell size <20 μm) and *H. minima*, which made up 78.41% of the total dinoflagellate cells but only 3.18% of the total phytoplankton cells in 2012 (Supplementary Table S6). These dinoflagellates emerged after the diatom spring bloom around 24 April and after the second *G. delicatula* bloom.

The diatom and dinoflagellate taxa observed in the studied period belong to phytoplankton groups typically found in the Bay of Brest (e.g., Queguiner and Tréguer, 1984). Between 2011 and 2017, approx. 46% of the total diatom cells belonged to the genus *Chaetoceros* and nearly half of the recorded dinoflagellate cells to the genus *Gymnodinum* (49%). The predominance of either diatoms or dinoflagellates was largely influenced by the availability of nutrients in the water column, e.g., the concentration of silicic acid (Ragueneau et al., 2002). In both years, the formation of large diatom blooms, which likely altered silicic acid stocks, was followed by the growth of non-siliceous dinoflagellates (Fig. 4C, D). The observed sea surface temperature (SST) varied between 8.7° (February) and 17.4 °C (September) in 2011 and between 9.8° (February) and 18.5 °C (August) in 2012 (Fig. 3C, D). In both years, the temperature stayed mostly below 12.5 °C prior to the first observed Ba/Ca_{shell} peak (Table 2), whereas the maximum temperature occurred after the last Ba/Ca_{shell} peak.

3.3. Time lag between phytoplankton blooms and Ba/Ca_{shell} peaks

Fourteen phytoplankton species of 2011 were assigned to category 1 (Supplementary Table S2). For another 13 phytoplankton species of 2011, a temporal shift of the chronology resulted in a good agreement with the barium data, but not all phytoplankton peaks coincided perfectly with Ba/Ca_{shell} peaks (assigned to category 2; Supplementary Table S2). Eight phytoplankton species showed strongly elevated abundances more than 30 days before the first Ba/Ca_{shell} peak or after the last Ba/Ca_{shell} peak (category 3; Supplementary Table S2) and were thus not recorded in the Ba/Ca_{shell} profile. The remaining six species of 2011 did not show any running similarity with the barium data, even when different time shifts were tested (category 4; Supplementary Table S2). Similar results were achieved for 2012. Thirteen species fell into category 1 and ten species into category 2 (Supplementary Table S2). Blooms of 14 species occurred either one month before the first Ba/Ca_{shell} peak or after the last Ba/Ca_{shell} excursion (category 3; Supplementary Table S2). The remaining three species belonged to category 4 (Supplementary Table S2).

In both years, the lead time of two species relative to Ba/Ca_{shell} peaks was less than eight days (*C. didymus*, *Protoperidinium depressum* in 2011 and *Alexandrium* spp., *Chaetoceros danicus* in 2012; Fig. 7). For another fifteen (2011) and seventeen (2012) species, a lag by eight to twelve days (Fig. 7) was required to manually crossdate the phytoplankton time-series with Ba/Ca_{shell} curves. Time lags larger than twelve days were determined for ten species in 2011, with a maximum of 30 days, and four species in 2012, with a maximum of 26 days (Fig. 7). The

Table 3
Diatom and dinoflagellate species observed in 2011 and 2012 and their time lag between corresponding Ba/Ca_{shell} peaks.

Phytoplankton species	Taxon	2011	2012
		Time lag (days)	Time lag (days)
Chaetoceros didymus	Diatom	5	13
Chaetoceros spp.	Diatom	9	10
Dinophysis acuminata	Dinoflag.	26	10
Guinardia delicatula	Diatom	25	11
Guinardia flaccida	Diatom	8	11
Haslea wawrickae	Diatom	10	12
Lepidodinium chlorophorum	Dinoflag.	12	12
Pseudo-nitzschia pungens	Diatom	10	10
Pseudo-nitzschia seriata	Diatom	9	11
Rhizosolenia imbricata	Diatom	8	10
Thalassionema nitzschioides	Diatom	9	10
Thalassiosira spp.	Diatom	13	13
Tripos kofoidii	Dinoflag.	16	12

manual determination of a temporal lag was ambiguous for some phytoplankton species, e.g., in 2011, the temporally non-shifted bloom of *D. fragilissimus* occurred contemporaneously with the first Ba/Ca_{shell} peak as well as with the second Ba/Ca_{shell} peak after shifting the time-series about ten days.

For ten diatoms and three dinoflagellate genera, a temporal shift could be determined that allowed an inter-annual comparison between 2011 and 2012 (Table 3). Nine phytoplankton species show similar temporal offsets (with an error of ±3 days) ranging from eight to thirteen days (i.e., *Chaetoceros* spp., *Guinardia flaccida*, *Haslea wawrickae*, *Lepidodinium* cf. *chlorophorum*, *Pseudo-nitzschia pungens*, *P. seriata*, *Rhizosolenia imbricata*, *Thalassionema nitzschioides*, *Thalassiosira* spp.). Offsets of three genera differed more than eight days (Table 3).

3.4. Random sampling simulation

The Monte Carlo simulations revealed distinct, randomly approximated weighting factors for the various tested phytoplankton species (Fig. 8). In general, the obtained confidence intervals (95% confidence level) varied between 0.24% (*Chaetoceros* spp.) and 18.04% (*Haslea wawrickae*) in 2011, and 0.57% (*Thalassiosira* spp.) and 18.69% (*Haslea wawrickae*) in 2012. For both studied years, the highest weighting factor was determined for the diatom species *T. nitzschioides* and the lowest for the diatom genus *Chaetoceros* spp. The calculated confidence intervals decreased with decreasing weighting factors, whereas the largest ranges occurred at weighting factors around 0.5 (Fig. 8).

4. Discussion

In agreement with previous findings (Barats et al., 2009), sharp Ba/Ca_{shell} peaks were largely uncorrelated to chlorophyll *a* values, as well as to the total diatom and dinoflagellate abundance. However, the Ba/Ca_{shell} peaks showed a strong agreement with the occurrence of certain diatom and dinoflagellate species when a short time lag of 8 to 13 days was applied. Besides this temporal accordance, Monte Carlo simulations suggested that cells of the various diatom and dinoflagellate species are likely to be associated with different amounts of Ba that can be incorporated into the shell.

4.1. Relationship between shell barium enrichments, chlorophyll a and the diatom and dinoflagellate abundance

As demonstrated by the highly resolved data, no direct link exists between Ba/Ca_{shell} profile and chlorophyll *a* pigment concentration (Fig. 4B). In both studied years, Ba/Ca_{shell} patterns differed significantly from the chlorophyll *a* time-series. For example, the double peak in Ba/Ca_{shell} in May 2011 (Fig. 4A) was not associated with a similar pattern in the chlorophyll *a* data. Although three gradually decreasing peaks occurred in the chlorophyll *a* data as well as in the Ba/Ca_{shell} profile in 2012, no temporal coincidence existed among both time-series, even when leads and lags were considered. In 2011, the highest chlorophyll *a* concentration occurred ca. 90 days before the Ba/Ca_{shell} maximum (Fig. 4A, B). In contrast, in May 2012, the chlorophyll *a* concentration attained a high-stand ca. 80 days before the strongest shell Ba enrichment (Fig. 4A, B). The strongest correlation between the two time-series was obtained when the chlorophyll *a* time-series were shifted by 86 days and thus assuming that the signal transfer from the environment into the shell took ca. three months (Fig. 4B; right panel). However, this deduction seems unlikely. While the largest chlorophyll *a* and barium peaks agreed with each other, many smaller Ba/Ca_{shell} peaks could not be associated with chlorophyll *a* excursions, suggesting the larger correlation coefficient results from a bias. Due to the three-month offset between the two time-series, a much lower number of data points – specifically such of the few coinciding peaks – is used to compute the Pearson correlation coefficient. Furthermore, in previously published works different lags were observed between chlorophyll *a* and Ba/Ca_{shell} profiles of scallop shells. For example, in the study by Barats et al. (2009), the temporal offset between the timing of the chlorophyll *a* maximum and the largest Ba/Ca_{shell} peak varied strongly from year to year (ca. seven to 83 days). Gillikin et al. (2008) described a similarity between the overall chlorophyll *a* pattern and the Ba/Ca_{shell} peaks with an offset of 40 days, whereas Thébault et al. (2009) observed an offset of about one week in juvenile scallops of *Comptopallium radula*. It appears that the chlorophyll *a* maximum, which is usually associated with the phytoplankton spring bloom in the Bay of Brest, always occurs prior to the Ba/Ca_{shell} maximum, but with variable temporal offsets. Together with these findings, the data presented in the current study suggest no direct link between the chlorophyll *a* pigment concentration and the formation of Ba/Ca_{shell} maxima. However, it should be mentioned that the chlorophyll *a* concentration is not an ideal indicator for the total phytoplankton biomass (Desortová, 1981; Kruskopf and Flynn, 2006) as the chlorophyll *a* concentration is also affected by light and nutrient availability, algal composition and the physiological condition of the phytoplankton cells (Behrenfeld et al., 2005; Behrenfeld and Boss, 2006; Lee et al., 2020).

Time-series of the total amount of diatom cells in the water column differed between the studied sampling years (Fig. 4C). At first sight, a relationship between blooms of diatoms and the Ba/Ca_{shell} peaks cannot be determined. However, some similarities are evident: Firstly, the double peak associated with the spring bloom in 2011 also occurred in the Ba/Ca_{shell} time-series, but with an offset of about nine days. In addition, after a similar temporal lag of nine days, the largest diatom cell concentration that was observed in both years coincided with the smallest Ba/Ca_{shell} peak (Fig. 4A, C). In 2012, only a smaller diatom spring bloom was observed followed by two larger summer blooms that were synchronized with the third and fourth Ba/Ca_{shell} peak with an offset of about ten days (Fig. 4A, C). Despite these overlapping patterns, not all Ba/Ca_{shell} peaks can be adequately explained as a response to the total diatom cell counts, i.e., the fourth peak in 2011 and the first and second peaks in 2012. Moreover, the Ba/Ca_{shell} peaks appear to be unrelated to the magnitude of the diatom cell concentration. For example, the largest diatom bloom in 2011 was associated with the lowest Ba enrichment, whereas the largest Ba peak (in 2012) can solely be attributed to a smaller diatom bloom. These observations were supported by the correlation coefficient plots (Fig. 4C; right panel) suggesting no statistical relationship exists between the total amount of diatom cells in the water column and the formation of Ba/Ca_{shell} peaks.

In both years, the concentration of dinoflagellate cells is significantly smaller than that of diatoms (Fig. 4D), which is a common observation in the Bay of Brest (Del Amo et al., 1997). The dinoflagellate time-series revealed several cell count maxima throughout both years. This impedes the comparison between Ba/Ca_{shell} peaks and dinoflagellate blooms because an unambiguous bloom-to-Ba/Ca_{shell} peak assignment was difficult to obtain. The correlation coefficients (Fig. 4D) indicated

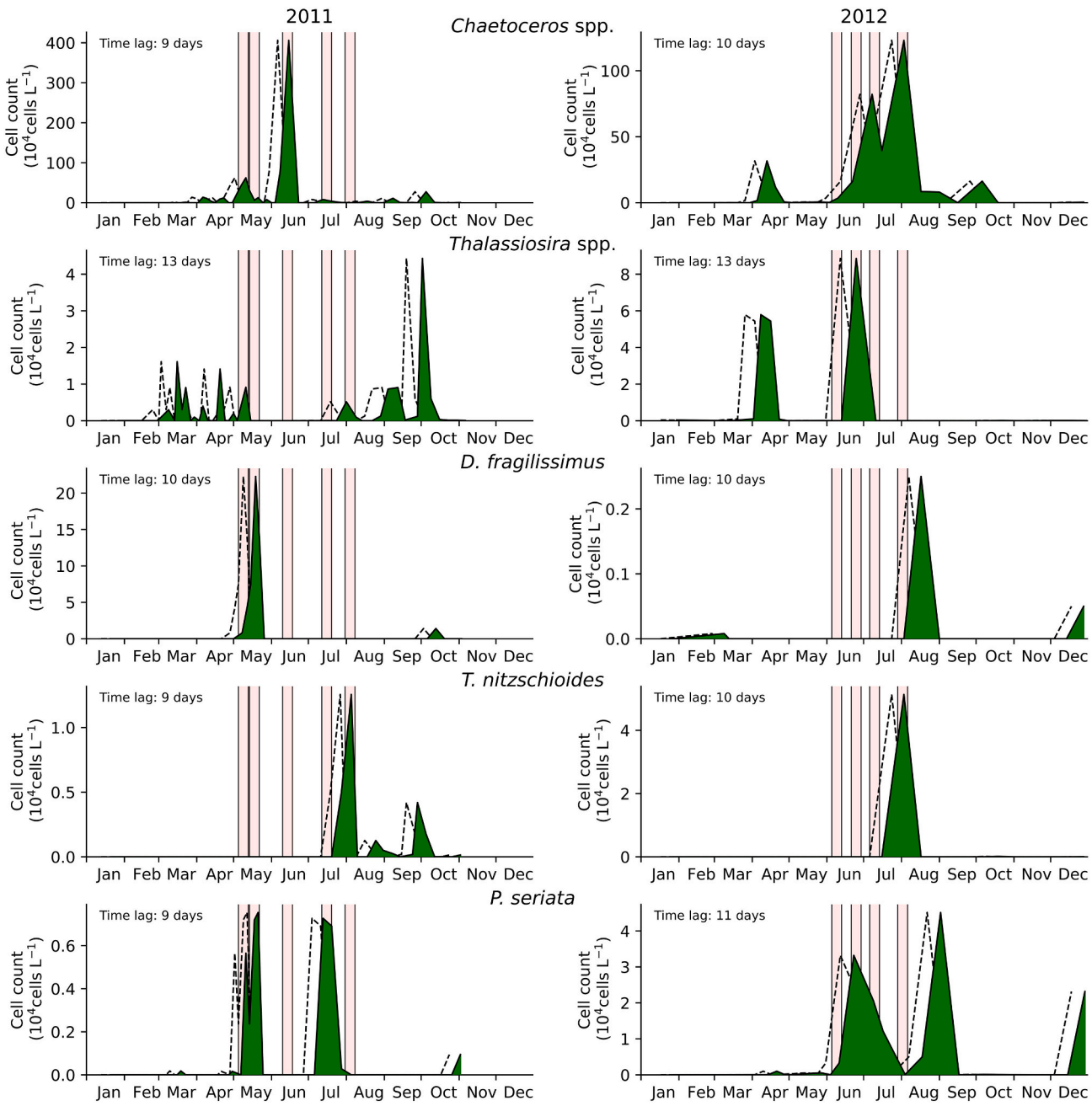

Fig. 6. Cell counts of five different diatom species at Lanvéoc during 2011 and 2012. The dashed line represents the original time of occurrence of each species, and the green area denotes the time-shifted diatom cell counts. To compare diatom cell peaks with Ba/Ca_{shell} peaks (red, vertical areas), a species-specific time lag (in days) was applied until the peaks agreed with each other. (For interpretation of the references to colour in this figure legend, the reader is referred to the web version of this article.)

that no significant correlation existed in both years when a similar time lag was applied. Thus, a causal relationship between the total cell concentration of dinoflagellates and Ba/Ca_{shell} peaks could not be verified.

The lack of similarity between the observed bulk phytoplankton dynamics and the Ba/Ca_{shell} peaks can likely be attributed to differences in the species composition of different chlorophyll *a*, diatoms, and dinoflagellate peaks (e.g., compare Fig. 4C and 5; each diatom peak differs in species composition). It was demonstrated that particle retention and subsequent ingestion in heterorhabdic bivalves (i.e., bivalves with gills containing two types of filaments), such as *P. maximus*, is not solely influenced by particle size (i.e., phytoplankton cell size) but is also affected by the nutritional value of the particles (Beninger et al., 2004; Chauvaud et al., 2001; Shumway et al., 1997; Ward and Shumway, 2004). This selective filter behavior supports the assumption that not all of the observed phytoplankton species, summarized in the bulk phytoplankton time-series, were consumed by the bivalves because the various taxa differed in cell size and nutritional value. In addition, different diatom species were shown to adsorb different amounts of barium leading to a variable vertical flux of this element toward the sediment water interface (SWI) (Dehairs et al., 1980; Fisher et al., 1991). In addition, environmental variables such as pH, iron supply and the dissolved Ba concentration in the water column affect the amount of phytoplankton cell-associated Ba that reaches the SWI (Sternberg et al., 2005). Accordingly, a species-specific comparison of individual phytoplankton genera and the timing of Ba/Ca_{shell} peaks is necessary to further disentangle a potential link between phytoplankton and barium

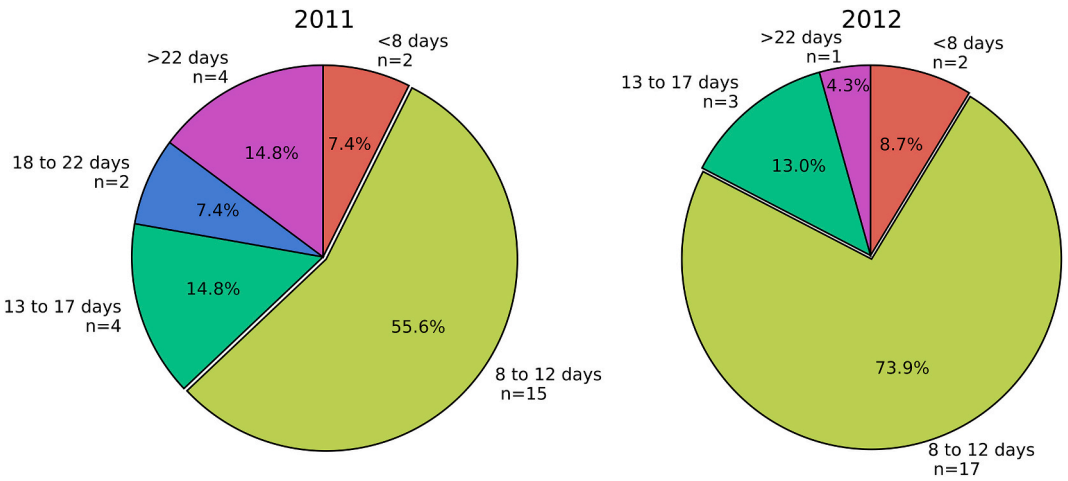

Fig. 7. The distribution of potential time lags (in days) that were determined for different diatom and dinoflagellate genera in 2011 (n = 27) and 2012 (n = 23).

peaks in the shell.

4.2. Ba/Ca_{shell} peaks and the timing of individual phytoplankton genera

In both studied years, most diatom blooms coincided with a subsequent formation of Ba/Ca_{shell} enrichments after a time lag of eight to twelve days, and only a few genera required larger or smaller theoretical temporal shifts to synchronize the peak patterns (Fig. 7, Supplementary Table S2). This observation is in accordance with the temporal offset determined for the total amount of diatom cells and the Ba/Ca_{shell} maxima (nine to ten days; section 4.1), as the total diatom cell concentration is largely influenced by a single diatom genus (Fig. 6; *Chaetoceros* spp.; this diatom group accounted for nearly 80% and 65% of the total diatom cells in 2011 and 2012, respectively). If the underlying hypothesis holds, i.e., that Ba/Ca_{shell} peaks are related to specific Ba-rich phytoplankton cells, Ba/Ca_{shell} peaks may not only be explained by blooms of the main diatom genus *Chaetoceros* spp., but also by blooms of less abundant diatoms species (when a time lag of a few days was applied). However, most of the dinoflagellate species do not provide an observable relationship between the cell concentration time-series and Ba/Ca_{shell} peaks (Supplementary Table S2).

The comparison between species-specific temporal lags obtained for both years (Table 3; Supplementary Table S2) allows to evaluate interannual similarities of individual phytoplankton species with the timing of Ba/Ca_{shell} peaks. Unfortunately, not all phytoplankton species present in 2011 also occurred in 2012, and vice versa (Supplementary Table S2). From the genera identified in both years, the blooms of nearly all species (except four) fitted best with Ba/Ca_{shell} peaks when a lag of 8 to 13 days was applied, with a small species-specific year-to-year difference of less than three days (Table 3). The heterogeneous patterns in the timing of Ba/Ca_{shell} peaks between 2011 and 2012, on the one hand, and the similarity of theoretically determined time lags, on the other hand, supports the assumption that a potential link exists between blooms of specific phytoplankton species (i.e., especially diatoms) and the incorporation of Ba into the shell. In other words, if there were no causal relationship between the timing of phytoplankton blooms and the occurrence of Ba/Ca_{shell} peaks it would be highly unlikely to expect similarities in the temporal lags between the two studied years (see Fig. 7).

4.3. Time lag

Although the Bay of Brest is a well-mixed ecosystem, the distribution of phytoplankton species varied between different sites (see Thébault and Chauvaud, 2013) and between bottom and surface waters. For instance, the main bloom of the diatom genus *Chaetoceros* near the sea surface was only recorded contemporaneously to a small extent at the SWI (see Supplementary Fig. S5). This vertically heterogenous phytoplankton distribution indicates that observed blooms in the upper water column do not occur simultaneously at the SWI. Consequently, a temporal offset has to be considered between the formation of a phytoplankton bloom at the surface and the time the cells require to reach the SWI where they are potentially ingested by filter feeders. Therefore, the time lag between a phytoplankton bloom and the subsequent formation of Ba/Ca_{shell} peaks is influenced by the sedimentation rate of the phytoplankton cells as well as the time it takes for Ba to be incorporated into the shell calcite after ingestion.

As shown in section 4.2, the shell Ba content lagged behind the majority of phytoplankton blooms by about 8 to 13 days (Fig. 7). The phytoplankton cell identifications were performed on water samples from 2 m below sea surface and the water depth at Lanvéoc is approx. 8 m. To reach the SWI within less than 8 to 13 days, phytoplankton cells have to sink, on average, 0.46 to 0.75 m d^{-1}. This sinking velocity is in the range observed for various phytoplankton species (Peperzak et al., 2003). However, it is shown that the sinking rate of phytoplankton cells does not correlate with the biovolume of the cells, but is rather influenced by the nutrient availability in the medium and by the colony density (Bienfang et al., 1982). Furthermore, aggregate forming diatoms exhibit a sinking velocity two orders of magnitude higher than that of unicellular diatoms (Alldredge and Gotschalk, 1989) leading to a rapid vertical flux of particles toward the SWI. In addition, the water depth strongly varies with the tide leading to a rapidly changing height of the water column throughout the year. These characteristics impede a theoretical approximation of a temporal lag solely based on constantly sinking particles from the upper part of the water column to the SWI.

Following Tabouret et al. (2012), Ba was enriched in the shell of *P. maximus* 6 to 8 days after an elevated level of dissolved Ba was measured in the ambient water. However, the sharp peaks in Ba/Ca_{shell} are potentially induced by the ingestion of phytoplankton cells containing Ba (Thébault et al., 2009) rather than dissolved Ba in the water column (Barats et al., 2009; Gillikin et al., 2008; Poitevin et al., 2020). The ingestion of Ba-rich phytoplankton cells is followed by a subsequent desorption of Ba in the digestive tract induced by the low gut pH. This results in larger amounts of Ba^{2+} reaching the site of shell formation (extrapallial space). Based on the high filtration rate of scallops (5 L h^{-1} g^{-1} dry weight) (Laing, 2004; Palmer, 1980), and the high biomineralization rates of *P. maximus* (Fig. 3A, B), especially after the first winter growth cessation, scallops could incorporate Ba into their shells rapidly. Therefore, it is reasonable to consider the observed temporal offset of 8 to 13 days in *P. maximus* as a potential time lag, although future studies about the species-specific sinking, digestion and incorporation rates of barium rich particles are needed to further prove such a lag. It should be

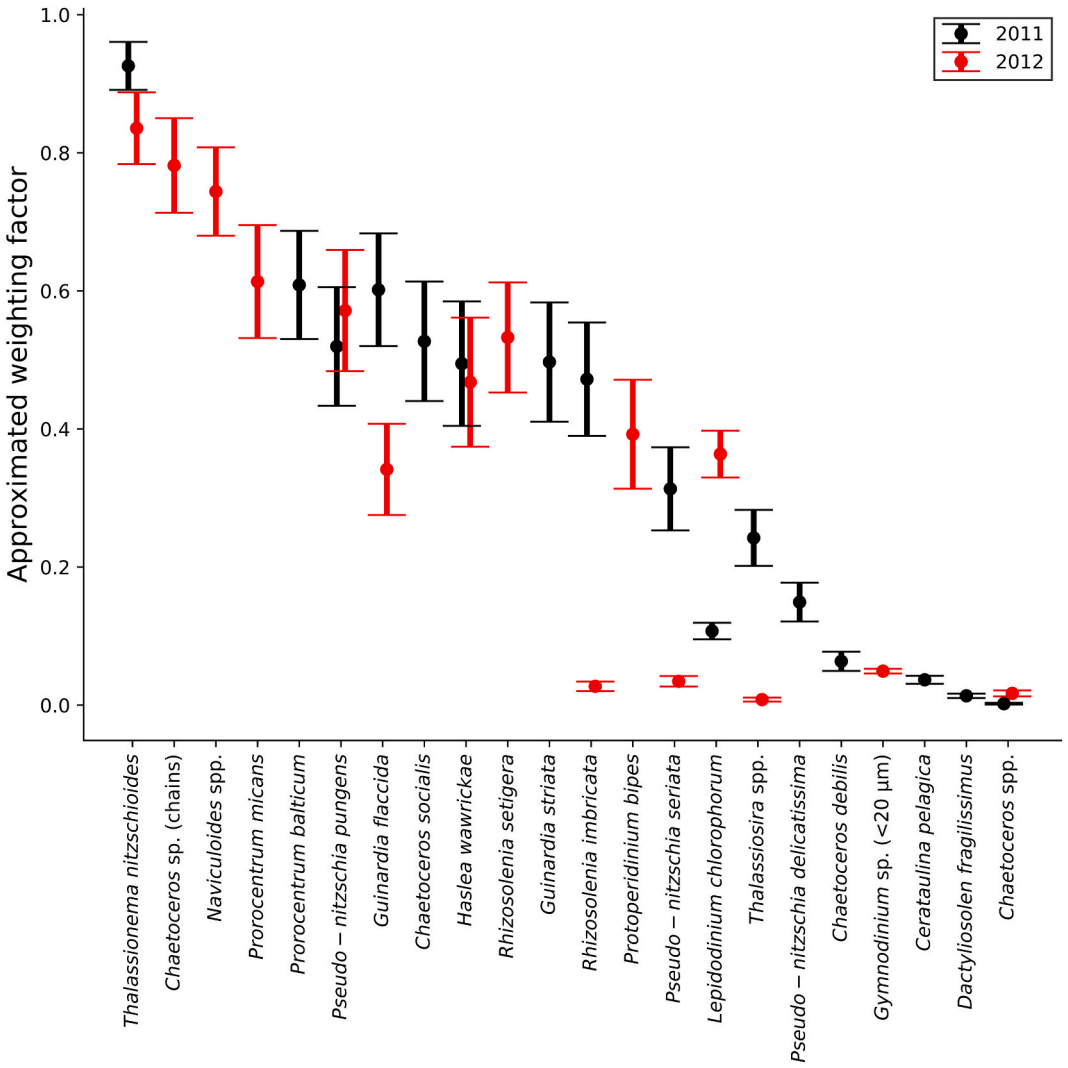

Fig. 8. 95% confidence intervals (circles indicate the corresponding mean) for different phytoplankton species calculated from 50 Monte Carlo experiments, including five billion simulations (see section 2.6), for 2011 and 2012. With a high probability, a certain weighting factor that describes the potential contribution of a phytoplankton species to the overall Ba/Ca_{shell} profile the best lies within the approximated weighting factor range that is determined for each species.

mentioned that there is a small uncertainty (± 2 days) given in the dating of the Ba/Ca_{shell} profiles and in the exact timing of phytoplankton cell peaks. Here, the measured maximum cell concentration of a respective bloom was used to determine the initial timing of the bloom. However, the actual bloom eventually arose shortly before or after the sampling (this can be concluded from the slight asymmetrical shape of the phytoplankton abundance peaks; see Fig. 6).

4.4. *Magnitude of Ba/Ca_{shell} peaks as a response to blooms of specific phytoplankton species*

As previously shown, the timing of most phytoplankton blooms that were observed in both years coincided with Ba/Ca_{shell} peaks considering a small temporal lag (see Table 3). However, if a direct link exists between the mass occurrence of certain phytoplankton species and the subsequent formation of Ba enrichments in the shell, the monitored cell concentrations did not serve as a suitable estimate for the amount of Ba that reached the site of shell formation, because the sum of cells of different phytoplankton time-series did not correlate well with the Ba/Ca_{shell} peak heights (Fig. 9). For example, the large abundance of the main diatom *Chaetoceros* spp. in 2011 coincided with the smallest Ba enrichment (Fig. 9; lower panel). Although peaks were temporally overlapping, the Ba/Ca_{shell} magnitude is not correlated with relative variations in the cell concentration. In addition, some blooms were not coinciding with Ba enrichments, in particular at the start of the growing season (see Fig. 6; blooms of *Thalassiosira* spp.). Therefore, even when considering a reasonable time lag, Ba/Ca_{shell} profiles cannot be reconstructed from the phytoplankton cell concentration time-series.

Three potential explanations for the observed discrepancies between the magnitude of Ba/Ca_{shell} peaks and cell concentrations are described as follows. (1) Temperature may affect the filtration activity of the bivalve (Laing, 2000, 2004). A gradual reduction in the filtration rate was determined for temperatures below 11 °C (Laing, 2004) which potentially hampers the formation of excessive Ba/Ca_{shell} peaks due to a reduced ingestion of Ba-rich particles. Although seawater temperature appears to have occasionally influenced the formation of Ba/Ca_{shell} peaks at the beginning of the growing season, when temperatures dropped below 12.5 °C (Fig. 3C, D), Barats et al. (2009) demonstrated that no significant correlation exists between Ba/Ca_{shell} ratios and SST. (2) The ability of the scallop gills to selectively filter particles out of the water column based on the particle size as well as the nutritional value (e.g., Beninger et al., 1992, 2004; Shumway et al., 1997) is likely to account for the observation that not all blooms of certain phytoplankton taxa could be assigned to Ba enrichments in the shell. Although this assumption does not apply for the discrepancies between blooms of the two diatom genera *Chaetoceros* and *Thalassiosira* and Ba/Ca_{shell} peaks

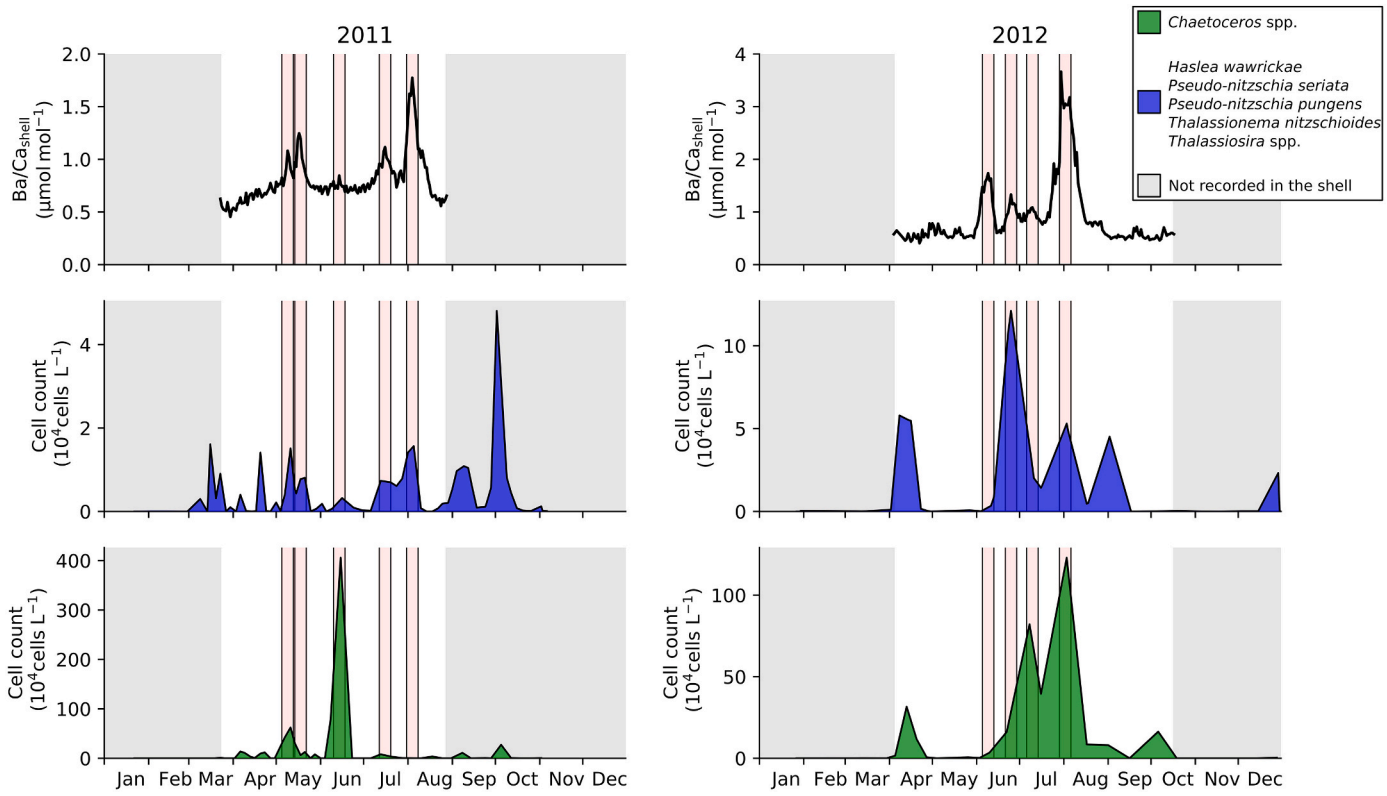

Fig. 9. Synchronicity of Ba/Ca$_{shell}$ peaks (1st subplot) and six diatom species after applying a species-specific time lag of 8 to 13 days. The blue area (2nd subplot) indicates the sum of the five diatoms referenced in the legend. To account for the exceedingly large abundance of *Chaetoceros* spp. cells in the studied years this species is displayed in an additional subplot (3rd subplot). (For interpretation of the references to colour in this figure legend, the reader is referred to the web version of this article.)

(see Fig. 6), as these diatoms were known to be consumed by *P. maximus* (Laing, 2004; Lorrain et al., 2000; Paulet et al., 1988), it may account for other phytoplankton species. (3) Environmental influences alter the phytoplankton cell-associated amount of Ba and/or species-specific differences in the ability to adsorb Ba. Following Sternberg et al. (2005), Ba is adsorbed onto iron oxyhydroxides on phytoplankton cell walls indicating that the ingestion and digestion of these Ba-rich cell walls account for the formation of Ba/Ca$_{shell}$ peaks (Thébault et al., 2009). As environmental conditions such as pH, iron and dissolved Ba concentration of the ambient seawater influence the amount of Ba linked to the cell walls (Fisher et al., 1991; Sternberg et al., 2005), these parameters should be taken into account when approximating the amount of Ba potentially reaching the site of biomineralization. Water pH did not vary strongly throughout 2011 and 2012 (average pH: 8.0 ± 0.1 in 2011 and 8.1 ± 0.1 in 2012) and was in the range described by Sternberg et al. (2005) to favor Ba adsorption onto phytoplankton cells. Unfortunately, iron and dissolved Ba concentration were not recorded in the studied years, but Barats et al. (2009) demonstrated that the dissolved Ba concentration is not correlated to the formation of transient Ba/Ca$_{shell}$ peaks. However, detailed environmental records are needed to better assess the relationship of plankton-associated Ba and Ba enrichments in scallop shells.

To further address the observed discrepancies in cell concentration and the magnitude of Ba/Ca$_{shell}$ peaks, a species-specific Ba enrichment factor was introduced, as previous studies reported a large variability in cell-associated Ba among various phytoplankton species (Dehairs et al., 1980; Fisher et al., 1991; Roth and Riley, 1971). First, it is hypothesized here that the cell surface area of the individual phytoplankton cells potentially serves as a rough estimator for the amount of Ba that can be attributed to a single cell, as demonstrated by Sternberg et al. (2005), Ba is adsorbed onto phytoplankton cell walls. However, testing this assumption did not provide adequate results, indicating that the surface area of individual phytoplankton species alone could not satisfactorily describe the relationship between the cell concentration and the magnitude of Ba/Ca$_{shell}$ peaks (see Supplementary Fig. S6). Therefore, another approach was considered to assess and quantify the contribution of specific phytoplankton species to the observed Ba/Ca$_{shell}$ profile, i.e., Monte Carlo simulations that randomly tested a huge number (five billion simulations per year) of different species-specific weighting combinations. This random sampling approach allowed to (1) weight each phytoplankton species individually, (2) calculate probability ranges that likely contain a deterministic best-fit weighting factor, (3) to draw species-specific conclusion and (4) to conduct an inter-annual comparison. The weights determined from these simulations (Fig. 8) represent species-specific approximations comprising and quantifying potential physiological and morphological variables (e.g., cell surface area, cell ornamentation, Si-content of the cell wall, microstructure of the cell wall, hydrous ferric oxide concentration of the cell surface) affecting the amount of Ba associated with a single cell.

The results (Fig. 8) demonstrate a clear pattern: Different phytoplankton species likely contribute differently to the Ba/Ca$_{shell}$ profiles, e.g., the largest weight was assigned to the diatom *T. nitzschioides* (Fig. 8). Individual cells of this species contribute more to the Ba content of the shell than cells of other species. Interestingly, this conclusion can be drawn from simulations independently performed for both studied years, which in turn, promotes the reliability of this random sampling approach. Since similar weights for both years were also obtained for other species, i.e., *P. pungens*, *Haslea wawrickae*, *Chaetoceros* spp. (Fig. 8), it is rather inappropriate to consider these results as simply random outcomes, although the approximations are based on random sampling. However, for some species larger inter-annual differences in weighting factors were obtained, i.e., *G. flaccida*, *R. imbricata*, *Pseudo-nitzschia*

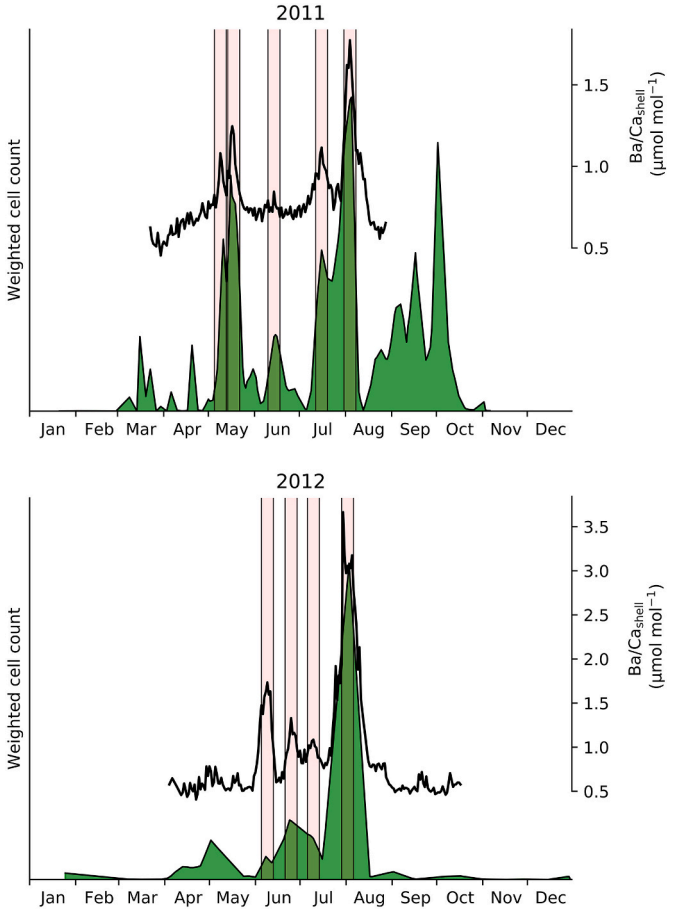

Fig. 10. The sum of cells of differently weighted phytoplankton species (green area), after a time lag of 8 to 13 days, for 2011 (16 species) and 2012 (15 species) and the respective Ba/Ca$_{shell}$ profiles. The species-specific factors were approximated by several Monte Carlo simulation (see section 2.6). The weighted cell counts are given in arbitrary units. (For interpretation of the references to colour in this figure legend, the reader is referred to the web version of this article.)

seriata, *Lepidodinium chlorophorum* and *Thalassiosira* spp. (Fig. 8; maximum difference of 45% between the mean weighting factors for *R. imbricata*). Accordingly, the influence of these species to the total Ba/Ca$_{shell}$ profile likely differed between the studied years. Since the approximation of the species-specific weights were based on simple assumptions (section 2.6), variable environmental factors likely affected the amount of cell-associated Ba, and potential differences in Ba assimilation rates contributed to the observed deviations among years. In addition, the simulations theoretically estimated the weighting factors while discarding a potential feeding preference of the scallops which could also account for inter-annual discrepancies observed for some phytoplankton taxa.

Many diatom species form large aggregates (Alldredge and Gotschalk, 1989), reaching several millimeters to centimeters in size, when the cells are physiologically stressed. These aggregates form at the end of an efflorescence and could cause gill clogging and a reduction in growth and filtration rates in scallops (e.g., Chauvaud et al., 1998; Lorrain et al., 2000). Likely, an increased amount of Ba is linked to polysaccharides exudated by flocculated diatoms (Alldredge et al., 1993; Martinez-Ruiz et al., 2018; Stecher and Kogut, 1999) which can support the formation of Ba/Ca$_{shell}$ peaks in scallop shells after ingestion of such aggregates. Accordingly, it should be hypothesized that aggregated diatoms can accumulate Ba to different amounts than single diatom cells.

Taking the species-specific weights and temporal lags (between 8 and 13 days) into account results in the time-series depicted in Fig. 10. These time-series compare well to the Ba/Ca$_{shell}$ profiles of the respective year and reveal relationships between different phytoplankton species and the Ba/Ca$_{shell}$ profile. Using this configuration, all Ba/Ca$_{shell}$ peaks can be explained with temporally lagged blooms of different phytoplankton species. Moreover, the magnitude of the shell Ba enrichments is approximated by weighting each bloom individually. Except for the first Ba/Ca$_{shell}$ peak in 2012 (Fig. 10), the relative magnitude of the Ba enrichments was well approximated. This can potentially be attributed to the fact that only diatoms and dinoflagellate species with cell concentrations larger than 1000 cells L^{-1}were included in this study. Furthermore, minor blooms or the overall sum of minor blooms could have also contributed to the Ba/Ca$_{shell}$ peak.

The proposed species-specific contribution to the Ba/Ca$_{shell}$ profile should be evaluated by actual measurements and quantified in future studies. Since blooms of diatoms are likely to induce shell Ba enrichments, a special focus of subsequent experiments should be placed on phytoplankton species and their potential to adsorb Ba onto their cells. Furthermore, potential differences in the Ba content between unicellular and aggregate forming species have to be evaluated. To refine the determination of digestible phytoplankton species and their barium load, the feeding behavior of scallops should also be further assessed. Since this study solely focused on diatom and dinoflagellate species, it will be inevitable to consider other taxonomic groups that can also affect the formation of Ba/Ca$_{shell}$ peaks. Concerning the methodology, to the best of our knowledge, this study constitutes the first attempt to include random sampling simulations to reconstruct geochemical information from bivalve shells from complex environmental records, such as phytoplankton time-series, providing a promising tool for future studies to detect potential patterns between environment and geochemistry.

5. Summary and conclusions

According to the findings presented herein, Ba/Ca$_{shell}$ peaks of *P. maximus* were most likely induced by blooms of specific phytoplankton taxa, especially diatoms. This assumption is based upon the following findings: (1) Neither the amount of chlorophyll *a* pigment concentration nor the total cell concentration of dinoflagellates can explain the Ba/Ca$_{shell}$ patterns. The total cell concentration of diatoms agreed only weakly with the barium signals, even when a temporal offset of nine to ten days was assumed. (2) Time lags between the occurrence of blooms of certain phytoplankton species and the timing of Ba/Ca$_{shell}$ peaks indicate that the shell Ba enrichments are related to the mass production of certain phytoplankton species. Actually, many species appeared eight to thirteen days prior to the formation of a Ba/Ca$_{shell}$ peak. (3) Not all phytoplankton species could be linked with Ba/Ca$_{shell}$ peaks, suggesting a capability of scallops to select which particles can be ingested. It is shown that the magnitude of the Ba/Ca$_{shell}$ peaks does not correlate with the concentration of identified cells in the water column. However, applying species-specific weighting factors results in a high degree of running similarity between the Ba/Ca$_{shell}$ and the weighted cell concentration time-series. Thus, a species-specific amount of frustule-associated Ba is likely. Ba/Ca$_{shell}$ profiles were associated with specific phytoplankton taxa. Therefore, the timing and magnitude of Ba/Ca$_{shell}$ peaks can potentially serve as a proxy for the dynamics of specific phytoplankton taxa. The species-specificity of Ba/Ca$_{shell}$ peaks limits the usability of Ba/Ca$_{shell}$ profiles as an indicator for the overall phytoplankton dynamics that prevailed in the water column. However, understanding this connection between edible phytoplankton species and Ba in shells could help to evaluate past phytoplankton community structures on a species level. Findings of the present study are important to further constrain the applicability of Ba/Ca$_{shell}$ of *P. maximus* and can potentially be extrapolated to other bivalve species.

Declaration of Competing Interest

The authors declare that they have no known competing financial interests or personal relationships that could have appeared to influence the work reported in this paper.

Acknowledgements

Special thanks go to Brigitte Stoll and Ulrike Weis from the Max Planck Institute for Chemistry (Mainz) for their help with the LA-ICP-MS measurements. We gratefully thank the SCUBA divers Erwan Amice, Thierry Le Bec, Isabelle Bihannic and Emilie Grossteffan for the sample collection and the crew of the research vessel Albert Lucas for organizing and leading the cruises. Furthermore, we thank Beatriz Beker and Gaspard Delebecq for preparing and processing all water samples and providing the important phytoplankton data. We are grateful for comments raised by two anonymous reviewers that helped to further improve and streamline the manuscript.

Funding

This study was made possible by a German Research Foundation (DFG) grant to BRS (SCHO 793/21) within the framework of the French-German collaborative research project HIPPO (HIgh-resolution Primary Production multiprOxy archives) funded jointly by the DFG and ANR (Agence Nationale de la Recherche).

Appendix A. Supplementary data

Supplementary data to this article can be found online at https://doi.org/10.1016/j.chemgeo.2022.120743.

References

Alldredge, A.L., Gotschalk, C.C., 1989. Direct observations of the mass flocculation of diatom blooms: characteristics, settling velocities and formation of diatom aggregates. Deep Sea Res. Part A Oceanogr. Res. Pap. 36, 159–171. https://doi.org/10.1016/0198-0149(89)90131-3.

Alldredge, A.L., Passow, U., Logan, B.E., 1993. The abundance and significance of a class of large, transparent organic particles in the ocean. Deep Sea Res. Part I Oceanogr. Res. Pap. 40, 1131–1140. https://doi.org/10.1097/00004669-199501000-00013.

Anderson, R.F., Winckler, G., 2005. Problems with paleoproductivity proxies. Paleoceanography 20, 1–7. https://doi.org/10.1029/2004PA001107.

Averyt, K.B., Paytan, A., 2004. A comparison of multiple proxies for export production in the equatorial Pacific. Paleoceanography 19, 1–14. https://doi.org/10.1029/2004PA001005.

Barats, A., Pécheyran, C., Amouroux, D., Dubascoux, S., Chauvaud, L., Donard, O.F.X., 2007. Matrix-matched quantitative analysis of trace-elements in calcium carbonate shells by laser-ablation ICP-MS: Application to the determination of daily scale profiles in scallop shell (*Pecten maximus*). Anal. Bioanal. Chem. 387, 1131–1140. https://doi.org/10.1007/s00216-006-0954-8.

Barats, A., Amouroux, D., Chauvaud, L., Pécheyran, C., Lorrain, A., Thébault, J., Church, T.M., Donard, O.F.X., 2009. High frequency Barium profiles in shells of the Great Scallop *Pecten maximus*: a methodical long-term and multi-site survey in Western Europe. Biogeosciences 6, 157–170. https://doi.org/10.5194/bg-6-157-2009.

Barton, S., Jenkins, J., Buckling, A., Schaum, C.E., Smirnoff, N., Raven, J.A., Yvon-Durocher, G., 2020. Evolutionary temperature compensation of carbon fixation in marine phytoplankton. Ecol. Lett. 23, 722–733. https://doi.org/10.1111/ele.13469.

Behl, S., Donval, A., Stiborb, H., 2011. The relative importance of species diversity and functional group diversity on carbon uptake in phytoplankton communities. Limnol. Oceanogr. 56, 683–694. https://doi.org/10.4319/lo.2011.56.2.0683.

Behrenfeld, M.J., Boss, E., 2006. Beam attenuation and chlorophyll concentration as alternative optical indices of phytoplankton biomass. J. Mar. Res. 64, 431–451. https://doi.org/10.1357/002224006778189563.

Behrenfeld, M.J., Boss, E., Siegel, D.A., Shea, D.M., 2005. Carbon-based Ocean productivity and phytoplankton physiology from space. Glob. Biogeochem. Cycles 19, 1–14. https://doi.org/10.1029/2004GB002299.

Beman, J.M., Arrigo, K.R., Matson, P.A., 2005. Agricultural runoff fuels large phytoplankton blooms in vulnerable areas of the ocean. Nature 434, 211–214. https://doi.org/10.1038/nature03370.

Beninger, P.G., Ward, J.E., MacDonald, B.A., Thompson, R.J., 1992. Gill function and particle transport in *Placopecten magellanicus* (Mollusca: Bivalvia) as revealed using video endoscopy. Mar. Biol. 114, 281–288. https://doi.org/10.1007/BF00349531.

Beninger, P.G., Decottignies, P., Rincé, Y., 2004. Localization of qualitative particle selection sites in the heterorhabdic filibranch *Pecten maximus* (Bivalvia: Pectinidae). Mar. Ecol. Prog. Ser. 275, 163–173. https://doi.org/10.3354/meps275163.

Bienfang, P.K., Harrison, P.J., Quarmby, L.M., 1982. Sinking rate response to depletion of nitrate, phosphate and silicate in four marine diatoms. Mar. Biol. 67, 295–302. https://doi.org/10.1007/BF00397670.

Bishop, J.K.B., 1988. The barite-opal-organic carbon association in oceanic particulate matter. Nature 332, 341–343. https://doi.org/10.1038/332341a0.

Cadée, G.C., Hegeman, J., 2002. Phytoplankton in the Marsdiep at the end of the 20th century; 30 years monitoring biomass, primary production, and *Phaeocystis* blooms. J. Sea Res. 48, 97–110. https://doi.org/10.1016/S1385-1101(02)00161-2.

Cardinale, B.J., Srivastava, D.S., Duffy, J.E., Wright, J.P., Downing, A.L., Sankaran, M., Jouseau, C., 2006. Effects of biodiversity on the functioning of trophic groups and ecosystems. Nature 443, 989–992. https://doi.org/10.1038/nature05202.

Carré, M., Bentaleb, I., Bruguier, O., Ordinola, E., Barrett, N.T., Fontugne, M., 2006. Calcification rate influence on trace element concentrations in aragonitic bivalve shells: Evidences and mechanisms. Geochim. Cosmochim. Acta 70, 4906–4920. https://doi.org/10.1016/j.gca.2006.07.019.

Chauvaud, L., Thouzeau, G., Paulet, Y.M., 1998. Effects of environmental factors on the daily growth rate of *Pecten maximus* juveniles in the Bay of Brest (France). J. Exp. Mar. Biol. Ecol. 227, 83–111. https://doi.org/10.1016/S0022-0981(97)00263-3.

Chauvaud, L., Jean, F., Ragueneau, O., Thouzeau, G., 2000. Long-term variation of the Bay of Brest ecosystem: Benthic-pelagic coupling revisited. Mar. Ecol. Prog. Ser. 200, 35–48. https://doi.org/10.3354/meps200035.

Chauvaud, L., Donval, A., Thouzeau, G., Paulet, Y.M., Nézan, E., 2001. Variations in food intake of *Pecten maximus* from the Bay of Brest (France): Influence of environmental factors and phytoplankton species composition. Acad. Sci. 324, 1–13.

Chauvaud, L., Thébault, J., Clavier, J., Lorrain, A., Strand, Ø., 2011. What's hiding behind ontogenetic δ13C variations in mollusk shells? New insights from the Great Scallop (*Pecten maximus*). Estuar. Coasts 34, 211–220. https://doi.org/10.1007/s12237-010-9267-4.

Cheshire, H., Thurow, J., Nederbragt, A.J., 2005. Late Quaternary climate change record from two long sediment cores from Guaymas Basin, Gulf of California. J. Quat. Sci. 20, 457–469. https://doi.org/10.1002/jqs.944.

Dehairs, F., Chesselet, R., Jedwab, J., 1980. Discrete suspended particles of barite and the barium cycle in the open ocean. Earth Planet. Sci. Lett. 49, 528–550.

Del Amo, Y., Quéguiner, B., Tréguer, P., Breton, H., Lampert, L., 1997. Impacts of high-nitrate freshwater inputs on macrotidal ecosystems. II. Specific role of the silicic acid pump in the year-round dominance of diatoms in the Bay of Brest (France). Mar. Ecol. Prog. Ser. 161, 225–237. https://doi.org/10.3354/meps161225.

Desortová, B., 1981. Relationship between chlorophyll-a concentration and phytoplankton biomass in several reservoirs in Czechoslovakia. Hydrobiology 66, 153–169. https://doi.org/10.20818/jfe.1981.100_21.

Doré, J., Chaillou, G., Poitevin, P., Lazure, P., Poirier, A., Chauvaud, L., Archambault, P., Thébault, J., 2020. Assessment of Ba/Ca in *Arctica islandica* shells as a proxy for phytoplankton dynamics in the Northwestern Atlantic Ocean. Estuar. Coast. Shelf Sci. 237 https://doi.org/10.1016/j.ecss.2020.106628.

Dymond, J., Collier, R., McManus, J., Honjo, S., Manganini, S., 1997. Can the aluminum and titanium contents of ocean sediments be used to determine the paleoproductivity of the oceans? Paleoceanography 12, 586–593. https://doi.org/10.1029/97PA01135.

Field, C.B., Behrenfeld, M.J., Randerson, J.T., Falkowski, P., 1998. Primary production of the biosphere: Integrating terrestrial and oceanic components. Science 281, 237–240. https://doi.org/10.1126/science.281.5374.237.

Fisher, N.S., Guillard, R.R.L., Bankston, D.C., 1991. The accumulation of barium by marine phytoplankton grown in culture. J. Mar. Res. 49, 339–354. https://doi.org/10.1357/002224091784995882.

Ganeshram, R.S., François, R., Commeau, J., Brown-Leger, S.L., 2003. An experimental investigation of barite formation in seawater. Geochim. Cosmochim. Acta 67, 2599–2605. https://doi.org/10.1016/S0016-7037(03)00164-9.

Gillikin, D.P., Dehairs, F., Lorrain, A., Steenmans, D., Baeyens, W., André, L., 2006. Barium uptake into the shells of the common mussel (*Mytilus edulis*) and the potential for estuarine paleo-chemistry reconstruction. Geochim. Cosmochim. Acta 70, 395–407. https://doi.org/10.1016/j.gca.2005.09.015.

Gillikin, D.P., Lorrain, A., Paulet, Y.M., André, L., Dehairs, F., 2008. Synchronous barium peaks in high-resolution profiles of calcite and aragonite marine bivalve shells. Geo-Marine Lett. 28, 351–358. https://doi.org/10.1007/s00367-008-0111-9.

Hallmann, N., Schöne, B.R., Strom, A., Fiebig, J., 2008. An intractable climate archive - Sclerochronological and shell oxygen isotope analyses of the Pacific geoduck, *Panopea abrupta* (bivalve mollusk) from Protection Island (Washington State, USA). Palaeogeogr. Palaeoclimatol. Palaeoecol. 269, 115–126. https://doi.org/10.1016/j.palaeo.2008.08.010.

Hatch, M.B.A., Schellenberg, S.A., Carter, M.L., 2013. Ba/Ca variations in the modern intertidal bean clam *Donax gouldii*: an upwelling proxy? Palaeogeogr. Palaeoclimatol. Palaeoecol. 373, 98–107. https://doi.org/10.1016/j.palaeo.2012.03.006.

Henson, S.A., Sarmiento, J.L., Dunne, J.P., Bopp, L., Lima, I., Doney, S.C., John, J., Beaulieu, C., 2010. Detection of anthropogenic climate change in satellite records of ocean chlorophyll and productivity. Biogeosciences 7, 621–640. https://doi.org/10.5194/bg-7-621-2010.

Herguera, J.C., 2000. Last glacial paleoproductivity patterns in the eastern equatorial Pacific: benthic foraminifera records. Mar. Micropaleontol. 40, 259–275. https://doi.org/10.1016/S0377-8398(00)00041-4.

Herguera, J.C., Berger, W.H., 1991. Paleoproductivity from benthic foraminifera abundance: Glacial to postglacial change in the West-Equatorial Pacific. Geology 19,

1173–1176. https://doi.org/10.1130/0091-7613(1991)019<1173:PFBFAG>2.3.CO;2.
Iglesias-Rodriguez, M.D., Halloran, P.R., Rickaby, R.E.M., Hall, I.R., Colmenero-Hidalgo, E., Gittins, J.R., Green, D.R.H., Tyrrell, T., Gibbs, S.J., Von Dassow, P., Rehm, E., Armbrust, E.V., Boessenkool, K.P., 2008. Phytoplankton calcification in a high-CO_2 world. Science 320, 336–340. https://doi.org/10.1126/science.1154122.
Jochum, K.P., Stoll, B., Herwig, K., Willbold, M., 2007. Validation of LA-ICP-MS trace element analysis of geological glasses using a new solid-state 193 nm Nd:YAG laser and matrix-matched calibration. J. Anal. At. Spectrom. 22, 112–121. https://doi.org/10.1039/b609547j.
Jochum, K.P., Weis, U., Stoll, B., Kuzmin, D., Yang, Q., Raczek, I., Jacob, D.E., Stracke, A., Birbaum, K., Frick, D.A., Günther, D., Enzweiler, J., 2011. Determination of reference values for NIST SRM 610-617 glasses following ISO guidelines. Geostand. Geoanal. Res. 35, 397–429. https://doi.org/10.1111/j.1751-908X.2011.00120.x.
Jochum, K.P., Garbe-Schönberg, D., Veter, M., Stoll, B., Weis, U., Weber, M., Lugli, F., Jentzen, A., Schiebel, R., Wassenburg, J.A., Jacob, D.E., Haug, G.H., 2019. Nano-powdered calcium carbonate reference materials: significant progress for microanalysis? Geostand. Geoanal. Res. 43, 595–609. https://doi.org/10.1111/ggr.12292.
Jolivet, A., Asplin, L., Strand, O., Thébault, J., Chauvaud, L., 2015. Coastal upwelling in Norway recorded in Great Scallop shells. Limnol. Oceanogr. 60, 1265–1275. https://doi.org/10.1002/lno.10093.
Kruskopf, M., Flynn, K.J., 2006. Chlorophyll content and fluorescence responses cannot be used to gauge reliably phytoplankton biomass, nutrient status or growth rate. New Phytol. 169, 525–536. https://doi.org/10.1111/j.1469-8137.2005.01601.x.
Laing, I., 2000. Effect of temperature and ration on growth and condition of king scallop (*Pecten maximus*) spat. Aquaculture 183, 325–334. https://doi.org/10.1016/S0044-8486(99)00262-8.
Laing, I., 2004. Filtration of king scallops (*Pecten maximus*). Aquaculture 240, 369–384. https://doi.org/10.1016/j.aquaculture.2004.02.002.
Lazareth, C.E., Vander Putten, E., André, L., Dehairs, F., 2003. High-resolution trace element profiles in shells of the mangrove bivalve *Isognomon ephippium*: a record of environmental spatio-temporal variations? Estuar. Coast. Shelf Sci. 57, 1103–1114. https://doi.org/10.1016/S0272-7714(03)00013-1.
Lee, J.H., Lee, W.C., Kim, H.C., Jo, N., Kim, K., Lee, D., Kang, J.J., Sim, B.R., Kwon, J. Il, Lee, S.H., 2020. Temporal and spatial variations of the biochemical composition of phytoplankton and potential food material (Fm) in Jaran Bay, South Korea. Water 12, 1–16. https://doi.org/10.3390/w12113093.
Lindahl, O., Belgrano, A., Davidsson, L., Hernroth, B., 1998. Primary production, climatic oscillations, and physico-chemical processes: the Gullmar Fjord time-series data set (1985-1996). ICES J. Mar. Sci. 55, 723–729. https://doi.org/10.1006/jmsc.1998.0379.
Liu, H., Kelly, M.S., Campbell, D.A., Fang, J., Zhu, J., 2008. Accumulation of domoic acid and its effect on juvenile king scallop *Pecten maximus* (Linnaeus, 1758). Aquaculture 284, 224–230. https://doi.org/10.1016/j.aquaculture.2008.07.003.
Longerich, H.P., Jackson, S.E., Günther, D., 1996. Laser ablation inductively coupled plasma mass spectrometric transient signal data acquisition and analyte concentration calculation. J. Anal. At. Spectrom. 11, 899–904. https://doi.org/10.1039/JA9961100899.
Lorenzen, C.J., 1966. A method for the continuous measurement of *in vivo* chlorophyll concentration. Deep. Res. Oceanogr. Abstr. 13, 223–227. https://doi.org/10.1016/0011-7471(66)91102-8.
Lorrain, A., Paulet, Y.M., Chauvaud, L., Savoye, N., Nézan, E., Guérin, L., 2000. Growth anomalies in *Pecten maximus* from coastal waters (Bay of Brest, France): Relationship with diatom blooms. J. Mar. Biol. Assoc. UK 80, 667–673. https://doi.org/10.1017/S0025315400002496.
Lorrain, A., Paulet, Y.M., Chauvaud, L., Dunbar, R.B., Mucciarone, D., Fontugne, M., 2004. $\delta^{13}C$ variation in scallop shells: increasing metabolic carbon contribution with body size? Geochim. Cosmochim. Acta 68, 3509–3519. https://doi.org/10.1016/j.gca.2004.01.025.
Marali, S., Schöne, B.R., Mertz-Kraus, R., Griffin, S.M., Wanamaker, A.D., Butler, P.G., Holland, H.A., Jochum, K.P., 2017a. Reproducibility of trace element time-series (Na/Ca, Mg/Ca, Mn/Ca, Sr/Ca, and Ba/Ca) within and between specimens of the bivalve *Arctica islandica* – a LA-ICP-MS line scan study. Palaeogeogr. Palaeoclimatol. Palaeoecol. 484, 109–128. https://doi.org/10.1016/j.palaeo.2016.11.024.
Marali, S., Schöne, B.R., Mertz-Kraus, R., Griffin, S.M., Wanamaker, A.D., Matras, U., Butler, P.G., 2017b. Ba/Ca ratios in shells of *Arctica islandica*—potential environmental proxy and crossdating tool. Palaeogeogr. Palaeoclimatol. Palaeoecol. 465, 347–361. https://doi.org/10.1016/j.palaeo.2015.12.018.
Marchais, V., Richard, J., Jolivet, A., Flye-Sainte-Marie, J., Thébault, J., Jean, F., Richard, P., Paulet, Y.M., Clavier, J., Chauvaud, L., 2015. Coupling experimental and field-based approaches to decipher carbon sources in the shell of the great scallop, *Pecten maximus* (L.). Geochim. Cosmochim. Acta 168, 58–69. https://doi.org/10.1016/j.gca.2015.07.010.
Martin, J.H., Knauer, G.A., 1973. The elemental composition of plankton. Geochim. Cosmochim. Acta 37, 1639–1653. https://doi.org/10.1016/0016-7037(73)90154-3.
Martinez-Ruiz, F., Jroundi, F., Paytan, A., Guerra-Tschuschke, I., Abad, M.D.M., González-Muñoz, M.T., 2018. Barium bioaccumulation by bacterial biofilms and implications for Ba cycling and use of Ba proxies. Nat. Commun. 9, 1–9. https://doi.org/10.1038/s41467-018-04069-z.
Palmer, R.E., 1980. Behavioral and rhythmic aspects of filtration in the bay scallop, *Argopecten irradians concentricus* (say), and the oyster, *Crassostrea virginica* (Gmelin). J. Exp. Mar. Biol. Ecol. 45, 273–295. https://doi.org/10.1016/0022-0981(80)90062-3.
Paulet, Y.M., Lucas, A., Gerard, A., 1988. Reproduction and larval development in two *Pecten maximus* (L.) populations from Brittany. J. Exp. Mar. Biol. Ecol. 119, 145–156. https://doi.org/10.1016/0022-0981(88)90229-8.
Peperzak, L., Colijn, F., Koeman, R., Gieskes, W.W.C., Joordens, J.C.A., 2003. Phytoplankton sinking rates in the Rhine region of freshwater influence. J. Plankton Res. 25, 365–383. https://doi.org/10.1093/plankt/25.4.365.
Poitevin, P., Chauvaud, L., Pécheyran, C., Lazure, P., Jolivet, A., Thébault, J., 2020. Does trace element composition of bivalve shells record utra-high frequency environmental variations? Mar. Environ. Res. 158 https://doi.org/10.1016/j.marenvres.2020.104943.
Queguiner, B., Tréguer, P., 1984. Studies on the phytoplankton in the Bay of Brest (Western Europe). seasonal variations in composition, biomass and production in relation to hydrological and chemical features (1981–1982). Bot. Mar. 27, 449–460. https://doi.org/10.1515/botm.1984.27.10.449.
Ragueneau, O., Chauvaud, L., Leynaert, A., Thouzeau, G., Paulet, Y.M., Bonnet, S., Lorrain, A., Grall, J., Corvaisier, R., Le Hir, M., Jean, F., Clavier, J., 2002. Direct evidence of a biologically active coastal silicate pump: Ecological implications. Limnol. Oceanogr. 47, 1849–1854. https://doi.org/10.4319/lo.2002.47.6.1849.
Richardson, K., Heilmann, J.P., 1995. Primary production in the Kattegat: past and present. Ophelia 41, 317–328. https://doi.org/10.1080/00785236.1995.10422050.
Richardson, C.A., Crisp, D.J., Runham, N.W., 1980. An endogenous rhythm in shell deposition in *Cerastoderma edule*. J. Mar. Biol. Assoc. UK 60, 991–1004. https://doi.org/10.1017/S0025315400042041.
Roth, I., Riley, J.P., 1971. The distribution of trace elements in some species of phytoplankton grown in culture. J. Mar. Biol. Assoc. UK 51, 63–72. https://doi.org/10.1017/S0025315400006457.
Schöne, B.R., 2008. The curse of physiology - challenges and opportunities in the interpretation of geochemical data from mollusk shells. Geo-Marine Lett. 28, 269–285. https://doi.org/10.1007/s00367-008-0114-6.
Shumway, S.E., Cembella, A.D., 1993. The impact of toxic algae on scallop culture and fisheries. Rev. Fish. Sci. https://doi.org/10.1080/10641269309388538.
Shumway, S.E., Cucci, T.L., Lesser, M.P., Bourne, N., Bunting, B., 1997. Particle clearance and selection in three species of juvenile scallops. Aquac. Int. 5, 89–99. https://doi.org/10.1007/BF02764790.
Shuter, B., 1979. A model of physiological adaptation in unicellular algae. J. Theor. Biol. 78, 519–552. https://doi.org/10.1016/0022-5193(79)90189-9.
Sigman, D.M., Boyle, E.A., 2000. Glacial/interglacial variations in atmospheric carbon dioxide. Nature 407, 859–869. https://doi.org/10.2143/TVG.60.19.1001996.
Smith, V.H., 2003. Eutrophication of freshwater and coastal marine ecosystems: a global problem. Environ. Sci. Pollut. Res. 10, 126–139. https://doi.org/10.1065/espr2002.12.142.
Stecher, H.A., Kogut, M.B., 1999. Rapid barium removal in the Delaware estuary. Geochim. Cosmochim. Acta 63, 1003–1012. https://doi.org/10.1016/S0016-7037(98)00310-X.
Stecher, H.A., Krantz, D.E., Lord, C.J., Luther, G.W., Bock, K.W., 1996. Profiles of strontium and barium in *Mercenaria mercenaria* and *Spisula solidissima* shells. Geochim. Cosmochim. Acta 60, 3445–3456. https://doi.org/10.1016/0016-7037(96)00179-2.
Sternberg, E., Tang, D., Ho, T.Y., Jeandel, C., Morel, F.M.M., 2005. Barium uptake and adsorption in diatoms. Geochim. Cosmochim. Acta 69, 2745–2752. https://doi.org/10.1016/j.gca.2004.11.026.
Tabouret, H., Pomerleau, S., Jolivet, A., Pécheyran, C., Riso, R., Thébault, J., Chauvaud, L., Amouroux, D., 2012. Specific pathways for the incorporation of dissolved barium and molybdenum into the bivalve shell: an isotopic tracer approach in the juvenile Great Scallop (*Pecten maximus*). Mar. Environ. Res. 78, 15–25. https://doi.org/10.1016/j.marenvres.2012.03.006.
Takesue, R.K., Bacon, C.R., Thompson, J.K., 2008. Influences of organic matter and calcification rate on trace elements in aragonitic estuarine bivalve shells. Geochim. Cosmochim. Acta 72, 5431–5445. https://doi.org/10.1016/j.gca.2008.09.003.
Thébault, J., Chauvaud, L., 2013. Li/Ca enrichments in great scallop shells (*Pecten maximus*) and their relationship with phytoplankton blooms. Palaeogeogr. Palaeoclimatol. Palaeoecol. 373, 108–122. https://doi.org/10.1016/j.palaeo.2011.12.014.
Thébault, J., Chauvaud, L., Clavier, J., Fichez, R., Morize, E., 2006. Evidence of a 2-day periodicity of striae formation in the tropical scallop *Comptopallium radula* using calcein marking. Mar. Biol. 149, 257–267. https://doi.org/10.1007/s00227-005-0198-8.
Thébault, J., Chauvaud, L., L'Helguen, S., Clavier, J., Barats, A., Jacquet, S., Pécheyran, C., Amouroux, D., 2009. Barium and molybdenum records in bivalve shells: Geochemical proxies for phytoplankton dynamics in coastal environments? Limnol. Oceanogr. 54, 1002–1014. https://doi.org/10.4319/lo.2009.54.3.1002.
Vander Putten, E., Dehairs, F., Keppens, E., Baeyens, W., 2000. High resolution distribution of trace elements in the calcite shell layer of modern *Mytilus edulis*: Environmental and biological controls. Geochim. Cosmochim. Acta 64, 997–1011. https://doi.org/10.1016/S0016-7037(99)00380-4.
Ward, J.E., Shumway, S.E., 2004. Separating the grain from the chaff: Particle selection in suspension- and deposit-feeding bivalves. J. Exp. Mar. Biol. Ecol. 300, 83–130. https://doi.org/10.1016/j.jembe.2004.03.002.
Westberry, T., Behrenfeld, M.J., Siegel, D.A., Boss, E., 2008. Carbon-based primary productivity modeling with vertically resolved photoacclimation. Glob. Biogeochem. Cycles 22, 1–18. https://doi.org/10.1029/2007GB003078.
Winder, M., Sommer, U., 2012. Phytoplankton response to a changing climate. Hydrobiologia 698, 5–16. https://doi.org/10.1007/s10750-012-1149-2.
Worm, B., Barbier, E.B., Beaumont, N., Duffy, J.E., Folke, C., Halpern, B.S., Jackson, J.B. C., Lotze, H.K., Micheli, F., Palumbi, S.R., Sala, E., Selkoe, K.A., Stachowicz, J.J.,

Watson, R., 2006. Impacts of biodiversity loss on ocean ecosystem services. Science 314, 787–790. https://doi.org/10.1126/science.1132294.